Electronic Supplementary Information

Enantiopure chiroptical probes for circular dichroism and absorbance based detection of nerve gas simulant

Snehasish Debnath and Pabitra B. Chatterjee*

Analytical & Environmental Science Division and Centralized Instrument Facility,

CSIR-CSMCRI, G. B. Marg, Bhavnagar, Gujarat, India.

Academy of Scientific and Innovative Research (AcSIR),

CSIR-HRDC, Ghaziabad, Uttar Pradesh, India.

*Corresponding author: pbchatterjee@csmcri.res.in

Table of contents

Experimental section

Materials and Physical Measurements. 2,4-Dimethylphenol, (S)-(+)-2-amino-1-propanol, (R)-(-)-2-amino-1-propanol, (R)-(-)-2-amino-1-butanol, (S)-(+)-2-phenylglycinol, paraformaldehyde, vanadyl bis(acetylacetonate), vanadium oxytrichloride, 2-chloroethylethylsulfide (CEES), dimethylmethylphosphonate (DMMP), diethylmethylphosphonate (DEMP), 2-chloroethylethylether (CEE), triethylphosphite (TEP), bis(2-chloroethyl)aminehydrochloride (NM), diethylcyanophosphonate (DCNP), diethylchlorophosphate (DCP) bis(chloroethyl)ether (oxygen mustard, OM), and cellulose acetate were obtained from Aldrich and TCI. All solvents were acquired from finar and used without any further purification. The UV/vis spectra were recorded using Shimadzu 3600 UV-vis-NIR spectrophotometer and Varian Cary-500 UV-Vis spectrophotometer. Elemental analyses (C, H, and N) were performed on an Elementar Vario MICRO CUBE analyser. IR spectra were recorded using Agilent Technologies Cary 600 Series spectrometer using KBr pellet in the region 450-4000 cm^{-1}. ^{1}H, ^{13}C, and ^{51}V NMR were measured in FT-NMR (500 MHz) Advance II Bruker AV500 Essential. For ^{1}H and ^{13}C NMR experiments, TMS was used as internal standard. $VOCl_3$ in DCM was used as reference for ^{51}V NMR experiments. Single crystal X-ray diffraction analysis was performed using BRUKER SMART APEX (CCD) diffractometer. The ESI-MS was measured on Micromass Q-ToF microTM and Agilent technologies 6545 QTOF LCMS. The melting points of the ligands were measured using a Mettler-Toledo FP-62 instrument. The CD spectra were obtained using a JASCO CD spectropolarimeter (J-815) with a 150 W Xe arc lamp at 25 ℃. The CD analysis was performed between 700 and 250 nm with a standard sensitivity of 100 mdeg, using a bandwidth of 1 nm, a scanning speed of 500 nm/min, data pitch of 0.2 nm. Samples for UV/vis-CD experiments were taken in 1 cm thick quartz cuvette. Freiberg Instrument Miniscope MS-5000 bench top EPR/ESR X-band spectrometer with 9.8

GHz microwave frequency was used for performing EPR experiments. EPR experiments were conducted at 25 °C in acetonitrile using 20 mW microwave power and 0.2 mT modulation. For recording the videos 1 and 2, 1 mL acetonitrile solution of 50 µM (video 1) and 1 mM (video 2) probe were used separately. 1 mL 2 mM DCP (acetonitrile solution) was added separately to the probes' solutions. Next, EPR spectra were acquired immediately at 25 °C using 20 mW microwave power and 0.2 mT modulation. Samsung M51 smartphone has been used for capturing the videos 1 and 2 in the auto video mode. While, for recording the reaction time, in-built stopwatch of Samsung M31 smartphone has been used. XPS analysis was performed using Thermo Fisher Nexsa G2 Surface Analysis System.

Single crystal X-ray crystallography

Diffraction quality single crystal of H_3L_1 (block, colourless, 0.34 × 0.18 × 0.05 mm^3), H_3L_2 (rod, colourless, 0.55 x 0.34 x 0.08 mm^3), H_3L_4 (rod, colourless, 0.65 x 0.18 x 0.1 mm^3), 1 (plate, red, 0.42 × 0.22 × 0.05 mm^3), 2 (rectangular, brown, 0.323 × 0.184 × 0.06 mm^3), 3 (plate, red, 0.35 × 0.12 × 0.04 mm^3), and 4 (rectangular, brown, 0.93 x 0.16 x 0.06 mm^3) with suitable dimension were selected for data collection. Intensity data of H_3L_1, H_3L_2, H_3L_4, and compounds 1-4 were acquired at 298 (2) K, 100 (2) K, 100 (2) K, 295 (2) K, 100 (2) K, 295 (2) K, and 100 (2) K, respectively. A BRUKER SMART APEX diffractometer equipped with a CCD detector with MoKα radiation (λ=0.71073 Å) source was used for the data collection. Data collection was performed using ϕ and ω scan and no crystal decay was observed during the data collection. Summary of crystallographic data is compiled in Table S2 and S5. Accurate cell parameters and orientation matrices of the crystals were acquired from setting angles in the ranges 1.94 ≤ θ ≤ 26 containing 57042 reflections for H_3L_1, 1.94 ≤ θ ≤ 26 containing 23464 reflections for H_3L_2, 1.82 ≤ θ ≤ 26 containing 46616 reflections for H_3L_4, and 2.21 ≤ θ ≤ 25 containing 65837 reflections for 1, 2.53 ≤ θ ≤ 30.69 containing 136998 reflections for 2, 2.44 ≤ θ ≤ 30.6

containing 55930 reflections for 3, $2.26 \leq \theta \leq 32.08$ containing 30519 reflections for 4, respectively. After the data collection, empirical absorption corrections were carried out using the muti-scan and SADABS software.[1] For data collection and refinement, Bruker SMART software package was used. Bruker SAINT was employed for data integration and reduction.[2] The structures were solved by conventional direct methods and we refined on F^2 by a full matrix least squares with SHELXTL.[3] All non-hydrogen atoms were refined anisotropically based on all data minimizing $wR = [\Sigma[w((F_0^2 - F_c^2)^2]^{1/2}$, $R = \Sigma||F_0| - |F_c||/\Sigma|F_0|$ and $S = [\Sigma[w((F_0^2 - F_c^2)^2]/(n-p)]^{1/2}$. SHELXT 2018/2 and SHELXL-2018/3 were used for structure solution and structure refinement. ORTEP 3 was used for graphical purpose.[4]

Computational details

Using Gaussian 09 software package, calculations from density functional theory (DFT) were performed using mixed basis set B3LYP/6-311**G(2d,2p) for the C, H, N, O, P, and Cl and DFT/B3LYP employing LANL2DZ basis set for V atom.[5-13] The optimized geometries were further subjected to time-dependent density functional theory (TD-DFT) with same basis sets. Using ground state geometry as the starting point, the TD-DFT/CPCM method were performed to simulate the electronic transitions. Solution phase SCF energies of the optimized structures were calculated using the CPCM solvation model in acetonitrile.[14] Gaussview, Chemissian, and Gaussum were utilized to visualize the electron densities, MO energy levels, and electronic transitions.[15-17] The structures of DCP, DCNP, and DEMP were downloaded from PubChem and were optimized using basis set B3LYP/6-311**G(d,p).

General synthesis of the ligands H_3L_1–H_3L_4.

A mixture of enantiopure amino propanol (5 mmol) and paraformaldehyde (300 mg, 10 mmol) in 1:2 stoichiometry was dissolved in 15 mL ethanol and refluxed for ca. 1 h. Next, 2,4-

dimethylphenol (1.22 g, 10 mmol) was added into the reaction mixture and refluxed continuously under stirring for 3 days. Yellow oil was obtained after evaporation of the solvent in rotary evaporator, which was further triturated several times with petroleum ether to get solid ligands. Recrystallization of the solid from ethanol resulted crystalline ligands H_3L_1–H_3L_4 in pure form.

H_3L_1. [$C_{21}H_{29}NO_3$] (S)-6,6'-(((1-hydroxypropan-2-yl)azanediyl)bis(methylene))bis(2,4-dimethylphenol)

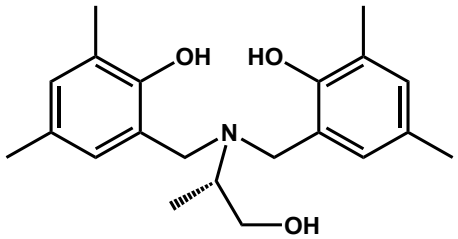

The amino propanol used for the preparation of H_3L_1 is (S)-(+)-2-amino-1-propanol (375 mg, 5 mmol). Yield: 38 % (recrystallized). MP: 118 °C. ^{1}H NMR ($CDCl_3$, 500 MHz, δ ppm): 6.84 (s, 2H), 6.69 (s, 2H), 4.10 (d, 2H, J=13.5 Hz), 3.77 (m, 2H, J=5.5 Hz), 3.25 (d, 2H, J=13.5 Hz), 3.27 (m, 1H), 2.18 (s, 6H), 2.19 (s, 6H), 0.93 (d, 3H, J=6.5 Hz). ^{13}C NMR ($CDCl_3$, 500 MHz, δ ppm) = 7.44, 15.95, 20.36, 50.88, 53.12, 63.9, 121.15, 124.91, 128.17, 128.51, 131.18, 151.21. Anal. Calcd. for $C_{63}H_{89}N_3O_{10}$: C, 72.11; H, 8.49; N, 4.01. Found: C, 71.63; H, 8.60; N, 3.95. ESI-MS (+ive, m/z): 344.22 $[M+H]^+$. Selected IR bands (cm^{-1}): 3332, 2912, 2862, 1610, 1484, 1442, 1376, 1306, 1243, 1208, 1154, 1047, 988, 860, and 769.

H_3L_2. [$C_{21}H_{29}NO_3$] (R)-6,6'-(((1-hydroxypropan-2-yl)azanediyl)bis(methylene))bis(2,4-dimethylphenol)

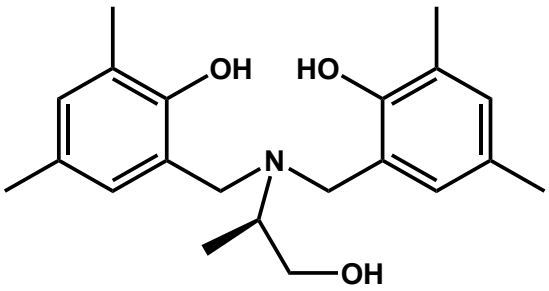

The amino propanol used for the preparation of H_3L_2 is (R)-(-)-2-amino-1-propanol (375 mg, 5 mmol). Yield: 45 % (recrystallized). MP: 120 °C. ^{1}H NMR ($CDCl_3$, 500 MHz, δ ppm): 6.84 (s, 2H), 6.69 (s, 2H), 4.14 (d, 2H, J=13 Hz), 3.76 (m, 2H), 3.25 (d, 2H, J=13.5 Hz), 3.12 (m, 1H), 2.19 (s, 6H), 2.17 (s, 6H), 0.93 (d, 3H, J=6.5 Hz). ^{13}C NMR ($CDCl_3$, 500 MHz, δ ppm) = 7.45, 15.95, 20.36, 50.87, 53.09, 63.85, 121.19, 124.88, 128.14, 128.50, 131.16, 151.81. Anal. Calcd. for $C_{63}H_{89}N_3O_{10}$: C, 72.11; H, 8.49; N, 4.01. Found: C, 72.63; H, 8.28; N, 3.99. ESI-MS (+ive, m/z): 344.22 $[M+H]^+$. Selected IR bands (cm^{-1}): 3332, 2945, 2828, 1615, 1486, 1444, 1379, 1302, 1243, 1208, 1152, 1049, 862, and 769.

H_3L_3. [$C_{22}H_{31}NO_3$] (R)-6,6'-(((1-hydroxybutan-2-yl)azanediyl)bis(methylene))bis(2,4-dimethylphenol)

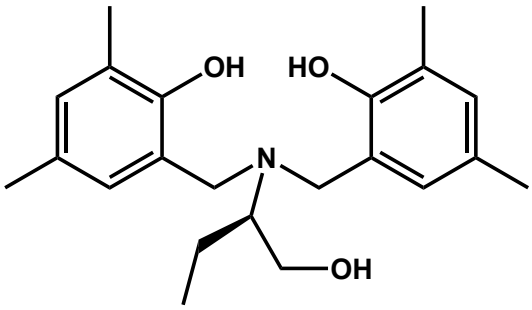

The amino propanol used for the preparation of H_3L_3 is (R)-(-)-2-amino-1-butanol (445 mg, 5 mmol). Yield: 40 % (recrystallized). MP: 78 °C. ^{1}H NMR ($CDCl_3$, 500 MHz, δ ppm): 6.83 (s, 2H), 6.67 (s, 2H), 4.27 (m, 1H), 4.10 (d, 2H, J=13. Hz), 3.83 (m, 2H), 3.29 (d, 2H, J=13.5 Hz), 2.82 (m, 1H), 2.17 (s, 6H), 2.19 (s, 6H), 1.8 (m, 1H), 1.26 (m, 1H), 0.84 (t, 3H, J=7.5 Hz). ^{13}C NMR ($CDCl_3$,

500 MHz, δ ppm) = 11.59, 15.97, 16.63, 20.37, 51.48, 59.46, 62.13, 121.48, 124.80, 126.80, 128.16, 128.58, 131.09, 151.86. Anal. Calcd. for $C_{66}H_{97}N_3O_{11}$: C, 71.45; H, 8.75; N, 3.79. Found: C, 72.73; H, 8.66; N, 3.88. ESI-MS (+ive, m/z): 358.24 $[M+H]^+$. Selected IR bands (cm^{-1}): 3316, 2937, 2870, 1612, 1486, 1376, 1208, 1154, 991, 862, 771, and 673.

H_3L_4. [$C_{26}H_{31}NO_3$] (S)-6,6'-(((2-hydroxy-1-phenylethyl)azanediyl)bis(methylene))bis(2,4-dimethylphenol)

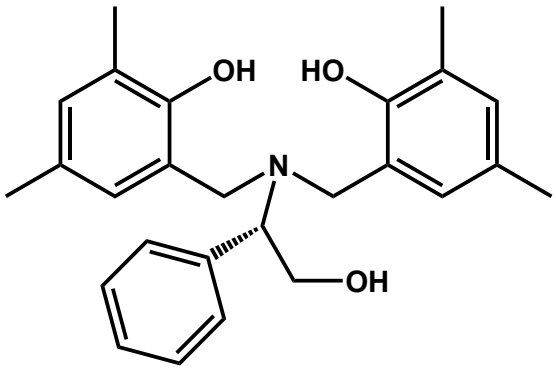

The amino propanol used for the preparation of H_3L_4 is (S)-(+)-2-Phenylglycinol (685 mg, 5 mmol). Yield: 36 % (recrystallized). MP: 158 °C. ^1H NMR ($CDCl_3$, 500 MHz, δ ppm): 7.39 (m, 3H), 7.18 (d, 2H, J=7.5 Hz), 6.86 (s, 2H), 6.59 (s, 2H), 4.4 (t, 1H, J=11.5 Hz), 4.24 (d, 2H, J=13 Hz), 4.10 (m, 1H), 3.92 (m, 1H, J=5.5 Hz), 2.97 (d, 2H, J=13.5 Hz), 2.20 (s, 6H), 2.18 (s, 6H). ^{13}C NMR ($CDCl_3$, 500 MHz, δ ppm) = 16.02, 20.38, 51.24, 61.46, 62.56, 120.86, 124.85, 128.22, 128.44, 128.75, 129.58, 131.21, 133.31, 151.92. Anal. Calcd. for $C_{56}H_{70}N_4O_7$: C, 73.76; H, 7.68; N, 6.15. Found: C, 73.14; H, 7.57; N, 6.37. ESI-MS (+ive, m/z): 406.23 $[M+H]^+$. Selected IR bands (cm^{-1}): 3282, 2929, 2853, 1484, 1449, 1238, 1215, 1154, 1115, 1021, 862, 766, and 698.

General synthesis of the oxovanadium(V) complexes 1-4.

Equimolar of H_3L_1–H_3L_4 and bis(acetylacetonato)oxovanadium(IV) (1 mmol) was taken in a round bottom flask and 15 mL acetonitrile was added to this mixture. The mixture was refluxed under stirring for 3-4 h. After completion of the reaction, brown crystalline solid was

obtained. Brown solid was collected by filtration and then air dried. Recrystallization from acetonitrile resulted compounds 1-4 in pure form.

Compound 1. [$C_{21}H_{26}NO_4V$]

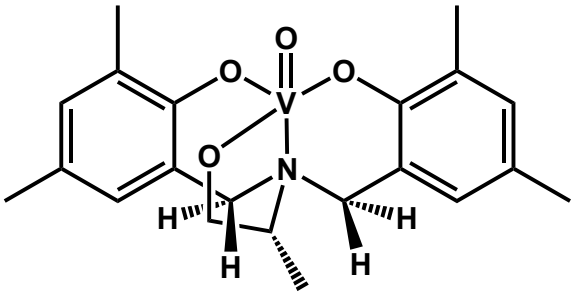

Yield: 73 % (recrystallized). ^{1}H NMR ($CDCl_3$, 500 MHz, δ ppm): 6.92 (s, 1H), 6.9 (s, 1H), 6.88 (s, 1H), 6.66 (s, 1H), 4.71 (t, 1H, J=13 Hz), 4.57 (d, 1H, J=13 Hz), 3.98 (d, 1H, J=13 Hz), 3.61 (d, 1H, J=14 Hz), 3.24 (m, 2H, J=5.5 Hz), 3.05 (m, 1H), 2.36 (s, 3H), 2.34 (s, 3H), 2.28 (s, 3H), 2.23 (s, 3H), 1.02 (d, 3H, J=6.5 Hz). ^{13}C NMR ($CDCl_3$, 600 MHz, δ ppm) = 6.04, 16.39, 20.67, 48.58, 53.05, 53.72, 81.65, 124.17, 124.28, 127.72, 128.23, 130.3, 130.4, 131.61, 132.51. ^{51}V NMR ($CDCl_3$, 500 MHz, δ ppm) = -389. Anal. Calcd. for $C_{21}H_{26}NO_4V$: C, 61.86; H, 6.38; N, 3.44. Found: C, 61.57; H, 6.52; N, 3.37. Selected IR bands (cm^{-1}): 2912, 2853, 1617, 1470, 1442, 1386, 1236, 1210, 1157, 1054, 1035, 953, 932, 850, 638, and 612. UV-vis (acetonitrile) [λ_{max}, nm (ε, Lmol^{-1}cm^{-1})]: 430 (11900) and 318 (8880).

Compound 2. [$C_{21}H_{26}NO_4V$]

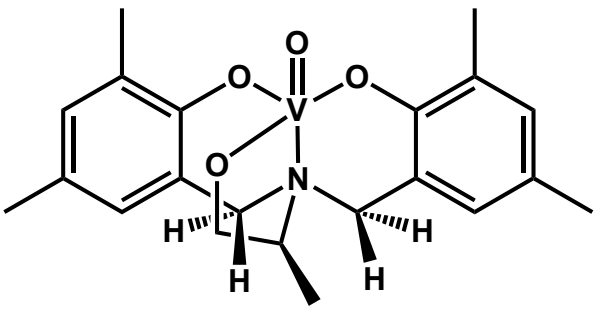

Yield: 71 % (recrystallized). ^{1}H NMR ($CDCl_3$, 500 MHz, δ ppm): 6.92 (s, 1H), 6.89 (s, 1H), 6.88 (s, 1H), 6.66 (s, 1H), 4.72 (t, 1H, J=11 Hz), 4.58 (t, 1H, J=11 Hz), 3.9 (d, 1H, J=13 Hz), 3.61 (d, 1H, J=14 Hz), 3.24 (m, 2H, J=4.5 Hz), 3.04 (m, 1H, J= 6 Hz), 2.36 (s, 3H), 2.34 (s, 3H), 2.28 (s, 3H), 2.23 (s, 3H), 1.02 (d, 3H, J=6.5 Hz). ^{13}C NMR ($CDCl_3$, 600 MHz, δ ppm) = 6.04, 16.44, 20.66, 48.56, 53.03, 53.71, 81.65, 124.16, 124.26, 124.62, 124.91, 127.70, 128.22, 130.28, 130.37, 131.59, 132.49, 163.72, 164.48. ^{51}V NMR ($CDCl_3$, 500 MHz, δ ppm) = -389. Anal. Calcd. for $C_{23}H_{29}N_2O_4V$: C, 61.55; H, 6.47; N, 6.24. Found: C, 61.90; H, 6.33; N, 6.37. Selected IR bands (cm^{-1}): 2912, 2853, 1470, 1444, 1381, 1367, 1236, 1213, 1159, 1056, 1038, 953, 930, 855, 787, 640, and 614. UV-vis (acetonitrile) [λ_{max}, nm (ε, $Lmol^{-1}cm^{-1}$)]: 430 (10200) and 310 (8200).

Compound 3. [$C_{22}H_{28}NO_4V$]

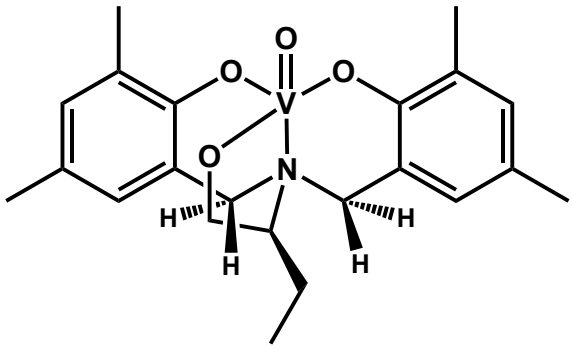

Yield: 64 % (recrystallized). ^{1}H NMR ($CDCl_3$, 500 MHz, δ ppm): 6.92 (s, 1H), 6.89 (s, 1H), 6.86 (s, 1Hz), 6.65 (s, 1Hz), 4.75 (m, 2H, J=11 Hz), 4.02 (d, 1H, J=13 Hz), 3.57 (d, 1H, J=13.5 Hz), 3.27 (m, 2H, J=13 Hz), 2.7 (m, 1H, J=3.5 Hz), 2.36 (s, 3H), 2.35 (s, 3H), 2.27 (s, 3H), 2.23 (s, 3H), 1.77 (m, 1H, J=3.5 Hz), 1.42 (m, 1H, J=3.5 Hz), 0.84 (t, 3H, J=7.5 Hz). ^{13}C NMR ($CDCl_3$, 500 MHz, δ ppm) = 11.58, 15.57, 16.38, 16.45, 20.68, 49.15, 53.03, 59.60, 80.44, 124.36, 124.38, 124.61, 124.75, 127.72, 128.19, 130.30, 130.36, 131.55, 132.47, 163.77, 164.36. ^{51}V NMR ($CDCl_3$, 500 MHz, δ ppm) = -388. Anal. Calcd. for $C_{22}H_{28}NO_4V$: C, 62.64; H, 6.64; N, 3.32. Found: C, 62.87; H, 6.79; N, 3.25. Selected IR bands (cm^{-1}): 2945, 2845, 1467, 1372, 1236, 1213, 1159, 1089,

1058, 1035, 954, 858, 750, 631, and 612. UV-vis (acetonitrile) [λ_{max}, nm (ε, $Lmol^{-1}cm^{-1}$)]: 430 (7200) and 310 (5940).

Compound 4. [$C_{26}H_{28}NO_4V$]

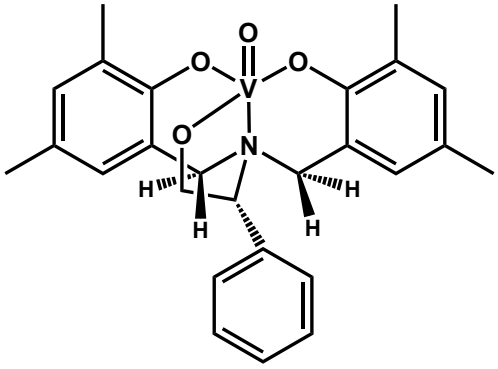

Yield: 68 % (recrystallized). ^1H NMR ($CDCl_3$, 500 MHz, δ ppm): 7.45 (t, 3H, J=3.5 Hz), 7.22 (t, 2H, J=3.5 Hz), 6.95 (s, 1H), 6.89 (s, 1H), 6.7 (d, 2H, J=7 Hz), 5.4 (t, 1H, J=12.5 Hz), 4.72 (m, 1H, J=5 Hz), 4.21 (d, 1H, J=12.5 Hz), 4.03 (m, 1H, J=6 Hz), 3.57 (d, 1H, J=14.5 Hz), 3.03 (d, 1H, J=14 Hz), 2.91 (d, 1H, J=12.5 Hz), 2.40 (s, 3H), 2.37 (s, 3H), 2.32 (s, 3H), 2.20 (s, 3H). ^{13}C NMR ($CDCl_3$, 500 MHz, δ ppm) = 16.4, 16.57, 20.56, 20.86, 50.01, 53.08, 62.44, 78.56, 124.23, 124.3, 124.5, 125.25, 128.17, 128.38, 128.63, 129.27, 129.74, 130.25, 130.3, 131.67, 132.8, 164.27, 164.95. ^{51}V NMR ($CDCl_3$, 500 MHz, δ ppm) = -395. Anal. Calcd. for $C_{28}H_{31}N_2O_4V$: C, 65.82; H, 6.07; N, 5.48. Found: C, 66.15; H, 6.19; N, 5.6. Selected IR bands (cm^{-1}): 2920, 2853, 1472, 1439, 1234, 1210, 1157, 1063, 1042, 963, 858, 706, 643, and 624. UV-vis (acetonitrile) [λ_{max}, nm (ε, $Lmol^{-1}cm^{-1}$)]: 430 (4760) and 315 (3800).

Casting of membrane for chiroptode preparation. The chiroptode compound 1CA was prepared according to the reported literature.[18] Cellulose acetate granules (1 g) were dissolved in 25 mL hot chloroform with constant stirring over a hot plate. 10 mL of 2.5 mM of 1 in chloroform solution was added dropwise to the cellulose acetate solution and stirred for

further 30 min. About 15 mL of this solution was spilled over a petri dish of 10 cm diameter. The freshly prepared membrane (compound 1CA) was kept overnight over the petri dish and allowed to dry at room temperature. Then it was separated out from the petri dish. The cellulose acetate membrane was cut into different sizes and preserved properly for detection of DCP vapour. The membrane was kept in vacuum for 1 h before its use.

General procedure for UV/vis and CD experiments using the chiroptode. The sensing experiment was carried out by hanging the chiroptode compound 1CA (cellulose acetate membrane casted with compound 1) in a 250 mL glass set up, with a thread. The flask was then heated to 150 ℃. 0.25 µL of DCP was then added to the bottom of the flask. The concentration of DCP vapor was estimated to be 1 ppm.[19] For UV-vis/CD experiments, the cellulose acetate membrane was cut into small pieces of 2x2 cm^2. The blank readings of the membrane were collected using membrane of cellulose acetate only. Next, spectra of the compound 1CA were also collected with and without exposure to DCP vapour.

To measure the concentration of the DCP vapour, we followed the method mentioned earlier in the literature.[19] Initially, we started with 40 ppm DCP vapour, which was prepared by taking 10 µL DCP in 250 mL flask. As expected, colour of the chiroptode changes from brown to colourless after few minutes of exposure. Next, we tested our probe separately with different concentrations of DCP vapour such as 20 ppm (5 µL DCP in 250 mL flask), 10 ppm (2.5 µL DCP in 250 mL flask), 5 ppm (1.25 µL DCP in 250 mL flask), and 1 ppm (0.25 µL DCP in 250 mL flask). In all cases, brown and CD-active chiroptode turned into colourless and CD silent.

General procedure for solution state UV/vis and CD experiments

Stock solutions (4 mM) of different organophosphorous compounds such as 2-chloroethylethylsulfide, dimethylmethylphosphonate, diethylmethylphosphonate, 2-chloroethylethylether, triethylphosphite, bis(2-chloroethyl)aminehydrochloride, 2-(dimethylamino)ethylchloridehydrochloride, diethylcyanophosphonate, diethylchlorophosphate, and bis(chloroethyl)ether were prepared in acetonitrile solution. Also, 100 µM stock solutions of 1-4 were prepared in acetonitrile. UV-vis and CD spectra were measured after the addition of 1 mL of respective analytes to 1 mL of 100 µM probe's solution. For comparison, control data were collected under identical conditions with blank solutions of 1-4 containing no DCP.

Determination of binding constant and limit of detection

The extent of binding of 1 towards DCP was calculated by linear fittings of the titration data using the following equation.

$$A_o/A = 1 + K[DCP]$$

A_o is the absorbance of 1 in absence of DCP and A is the absorbance of the product after the interaction of 1 with DCP. The value of K was determined from the linear fitting of the absorption titration curve.[20]

The detection limit was calculated on the basis of UV/vis and CD titration experiments of compound 1 with DCP in acetonitrile solution following the equation 3σ/k, where σ is the standard deviation of ten blank solutions (for 1 only) and k is absolute value of the slope of the intensity versus DCP concentration plot. The standard deviation was calculated by taking UV-vis and CD data of ten blank measurements. The values of the slope were obtained by

plotting the intensity against DCP concentrations at 430 nm (for UV-vis) and 415 nm (for CD), respectively.

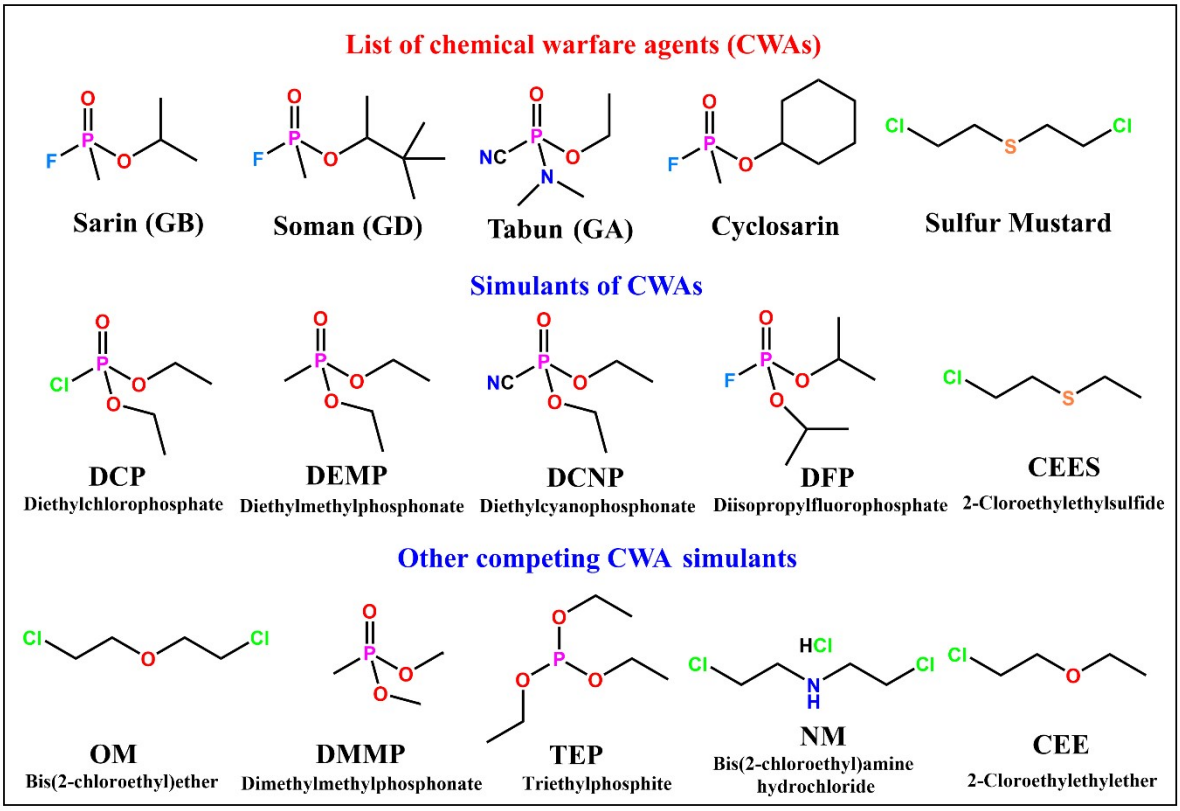

Scheme S1. List of chemical warfare agents (CWAs) along with their simulants.

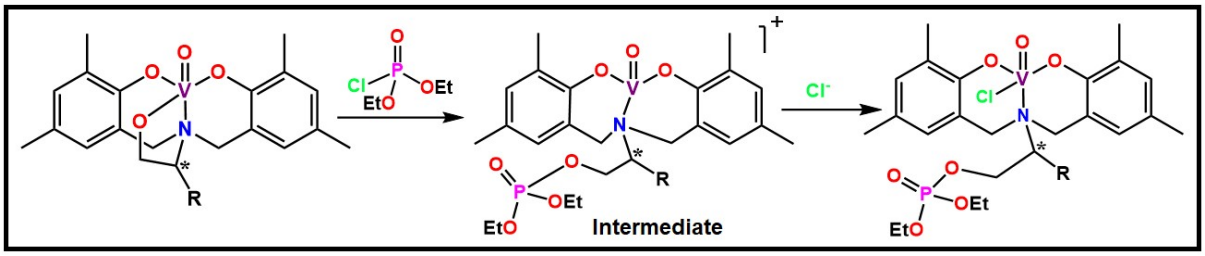

Scheme S2. Tentative mechanism of interaction between 1 and DCP.

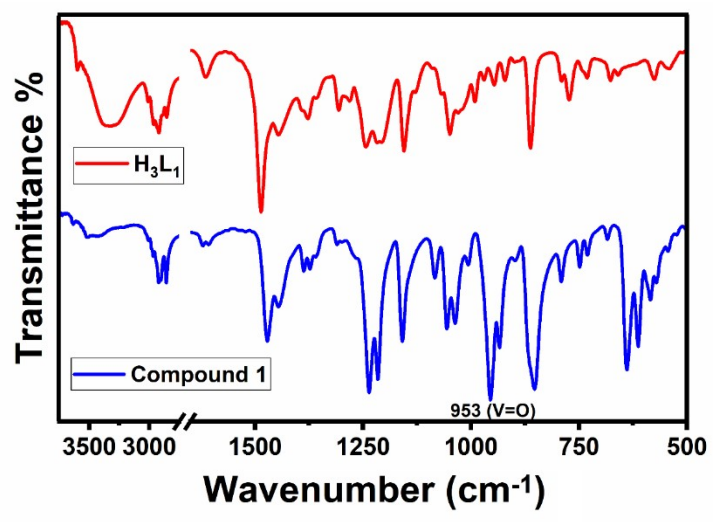

Fig. S1. FT-IR spectra of H_3L_1 (top panel) and its vanadium compound 1 (bottom panel).

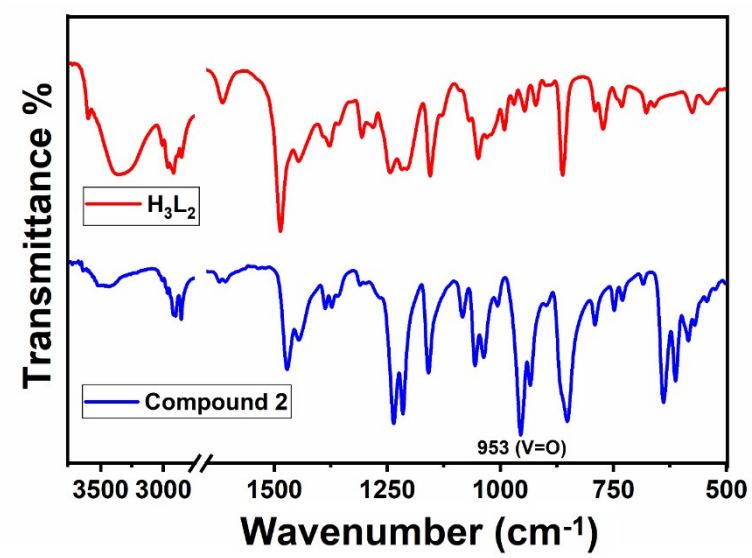

Fig. S2. FT-IR spectra of H_3L_2 (top panel) and its vanadium compound 2 (bottom panel).

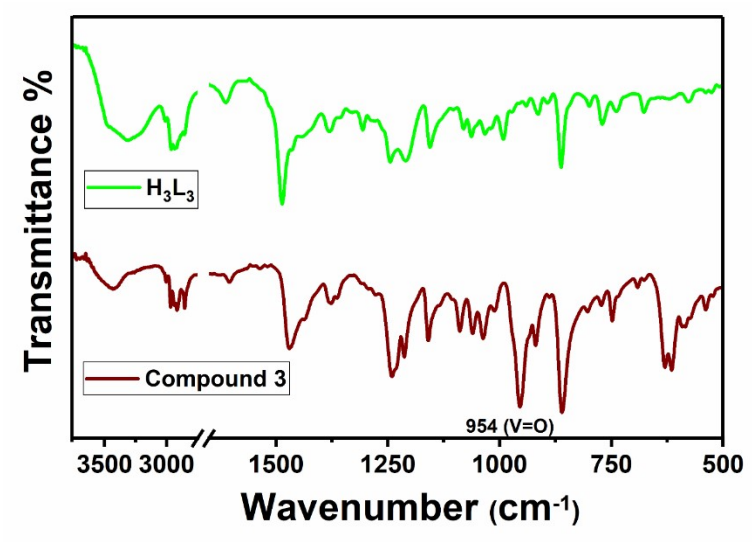

Fig. S3. FT-IR spectra of H_3L_3 (top panel) and its vanadium compound 3 (bottom panel).

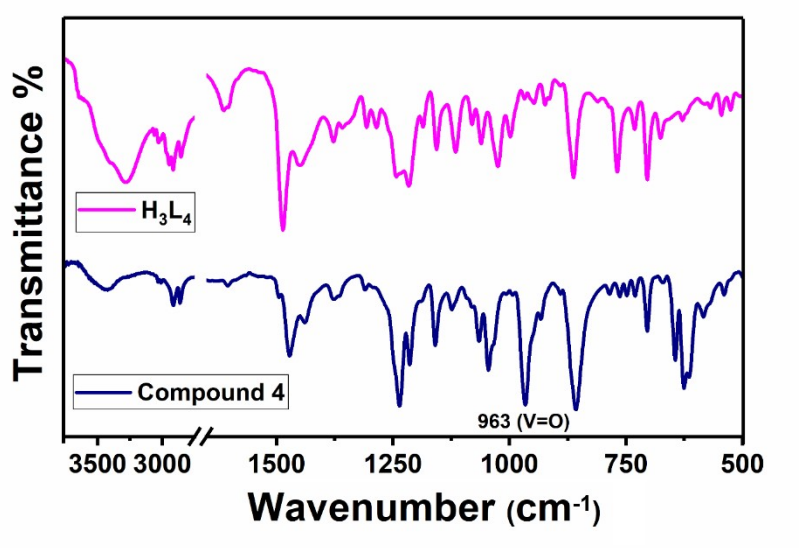

Fig. S4. FT-IR spectra of H_3L_4 (top panel) and its vanadium compound 4 (bottom panel).

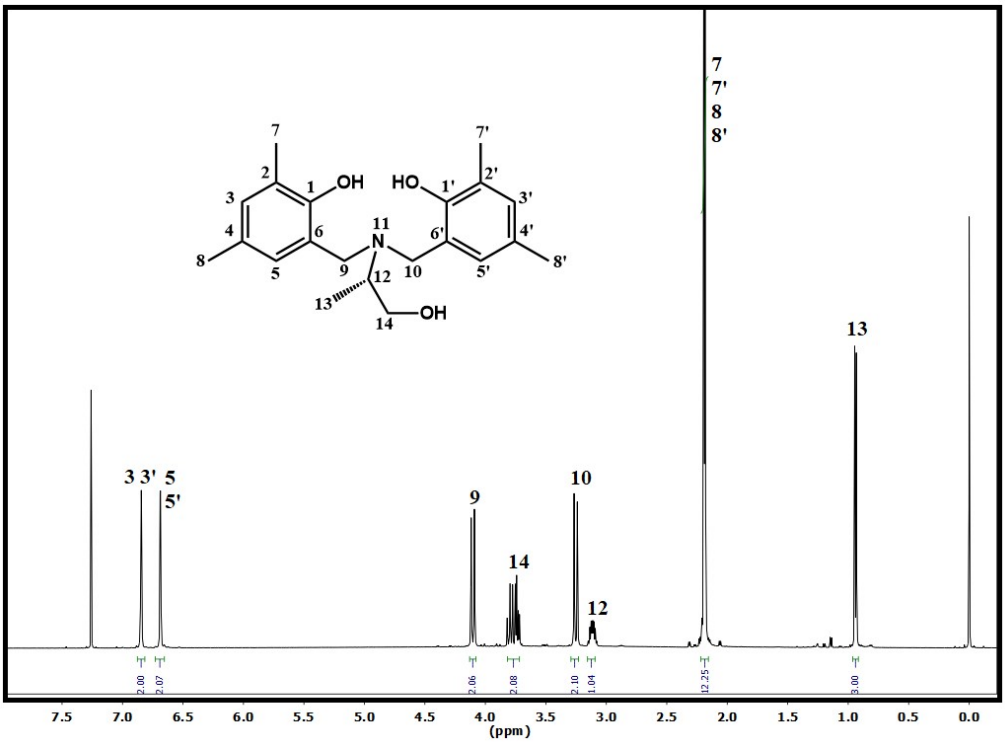

Fig. S5. ^{1}H NMR spectrum of H_3L_1 in $CDCl_3$.

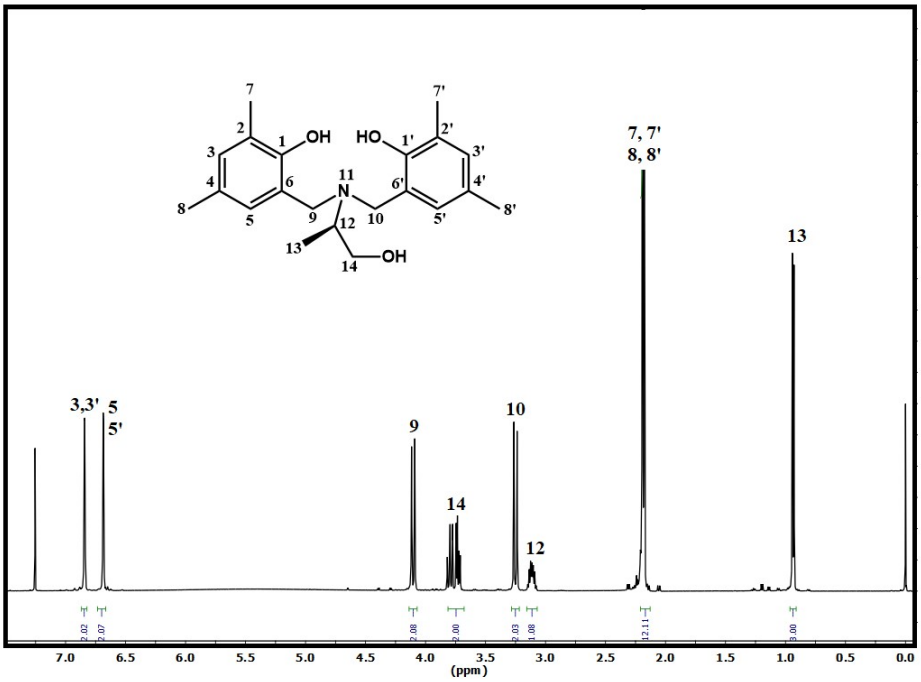

Fig. S6. ^{1}H NMR spectrum of H_3L_2 in $CDCl_3$.

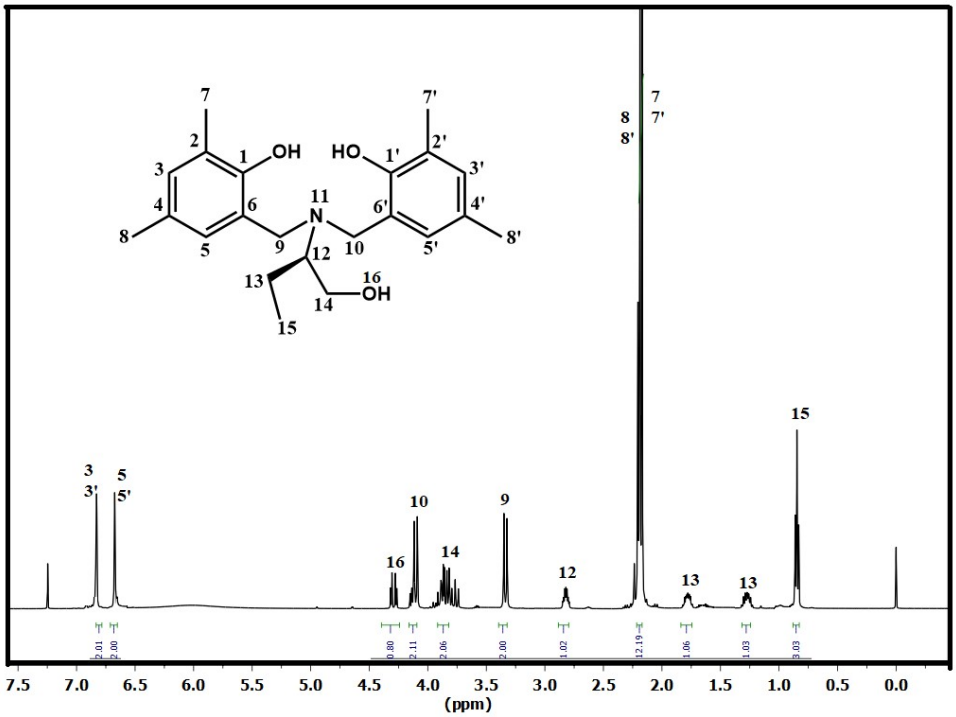

Fig. S7. ^{1}H NMR spectrum of H_3L_3 in $CDCl_3$.

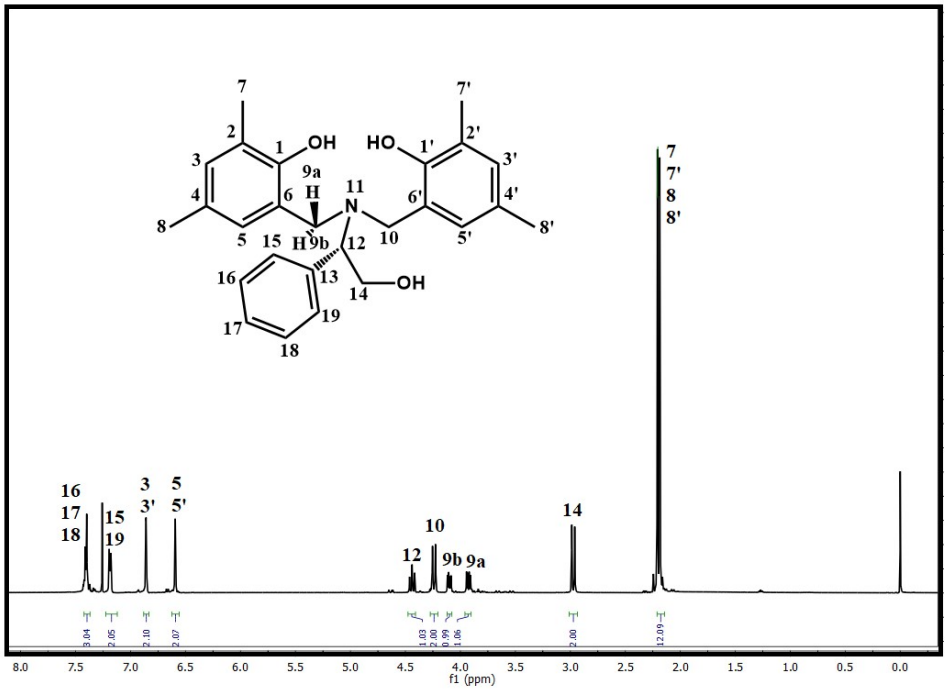

Fig. S8. ^{1}H NMR spectrum of H_3L_4 in $CDCl_3$.

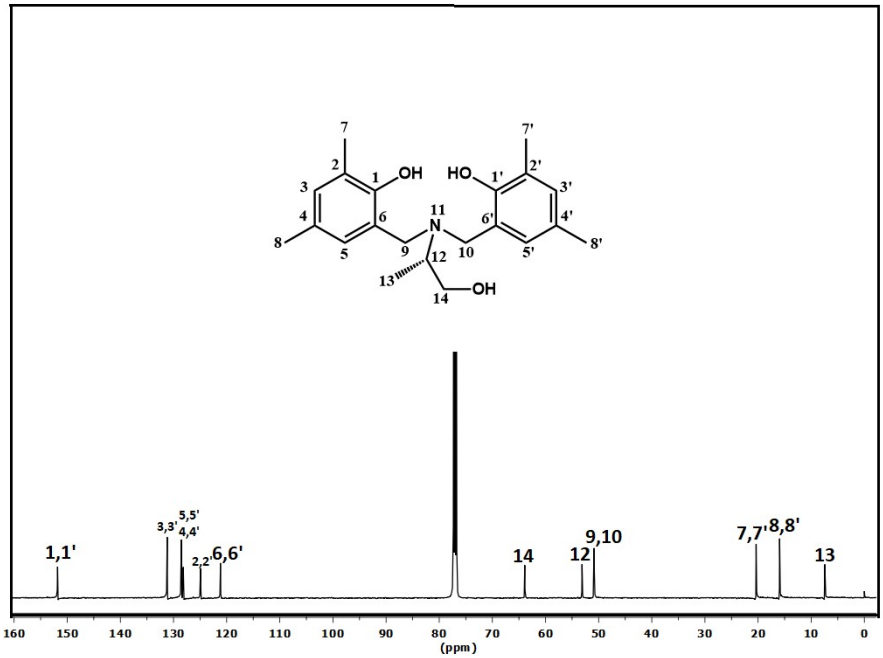

Fig. S9. ^{13}C NMR spectrum of H_3L_1 in $CDCl_3$.

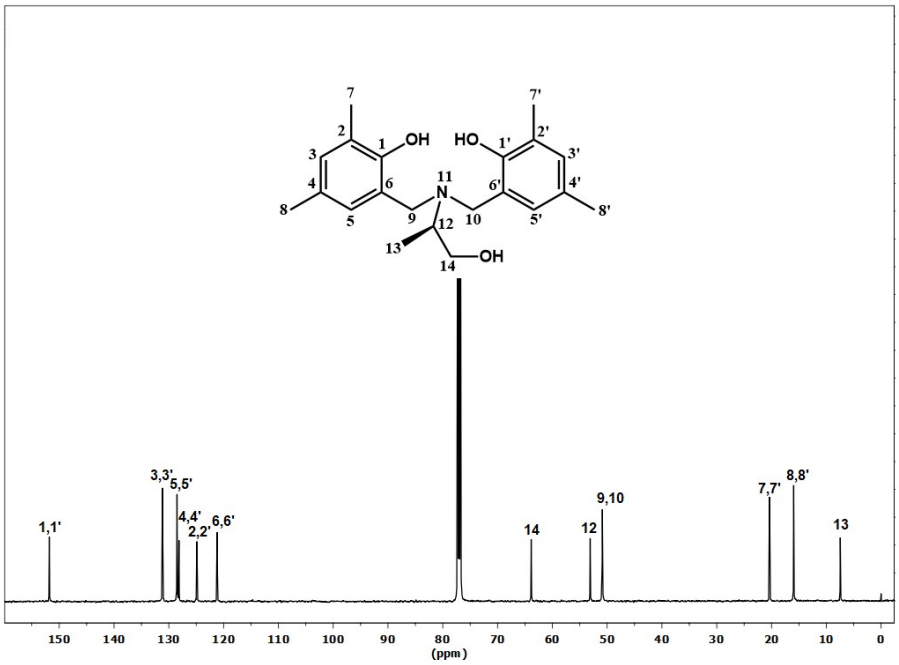

Fig. S10. ^{13}C NMR spectrum of H_3L_2 in $CDCl_3$.

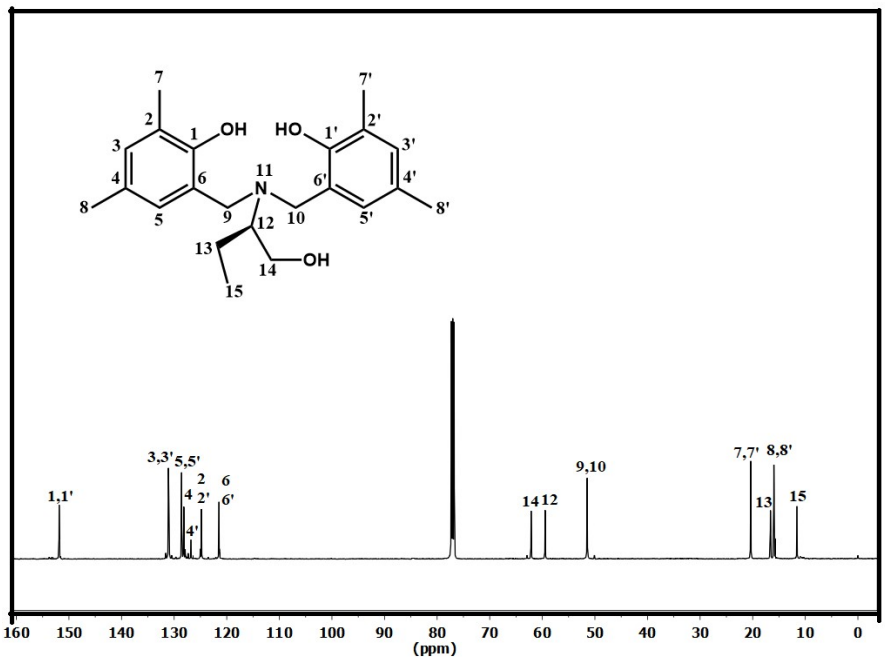

Fig. S11. ^{13}C NMR spectrum of H_3L_3 in $CDCl_3$.

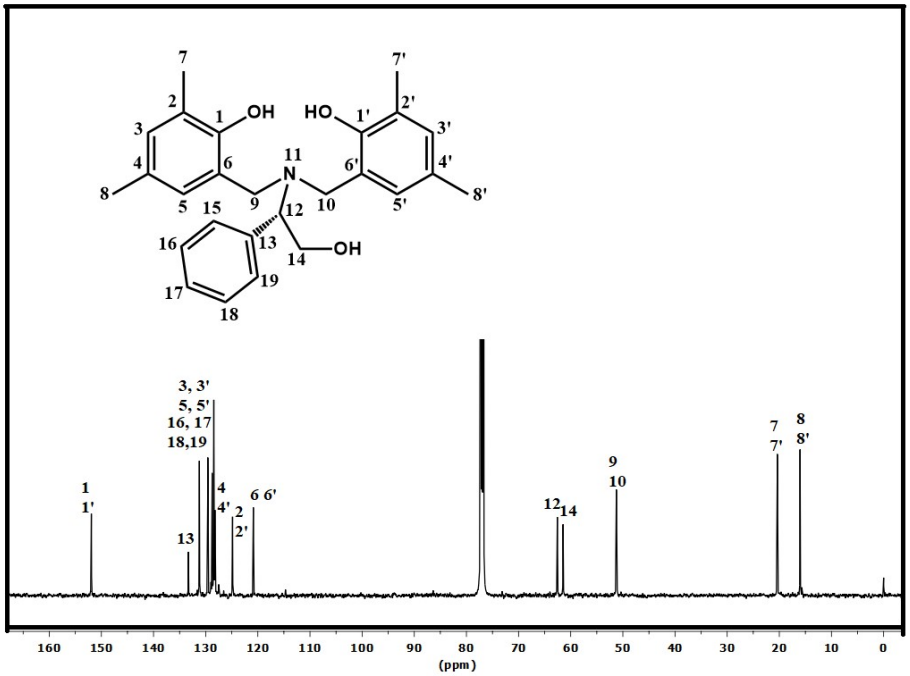

Fig. S12. ^{13}C NMR spectrum of H_3L_4 in $CDCl_3$.

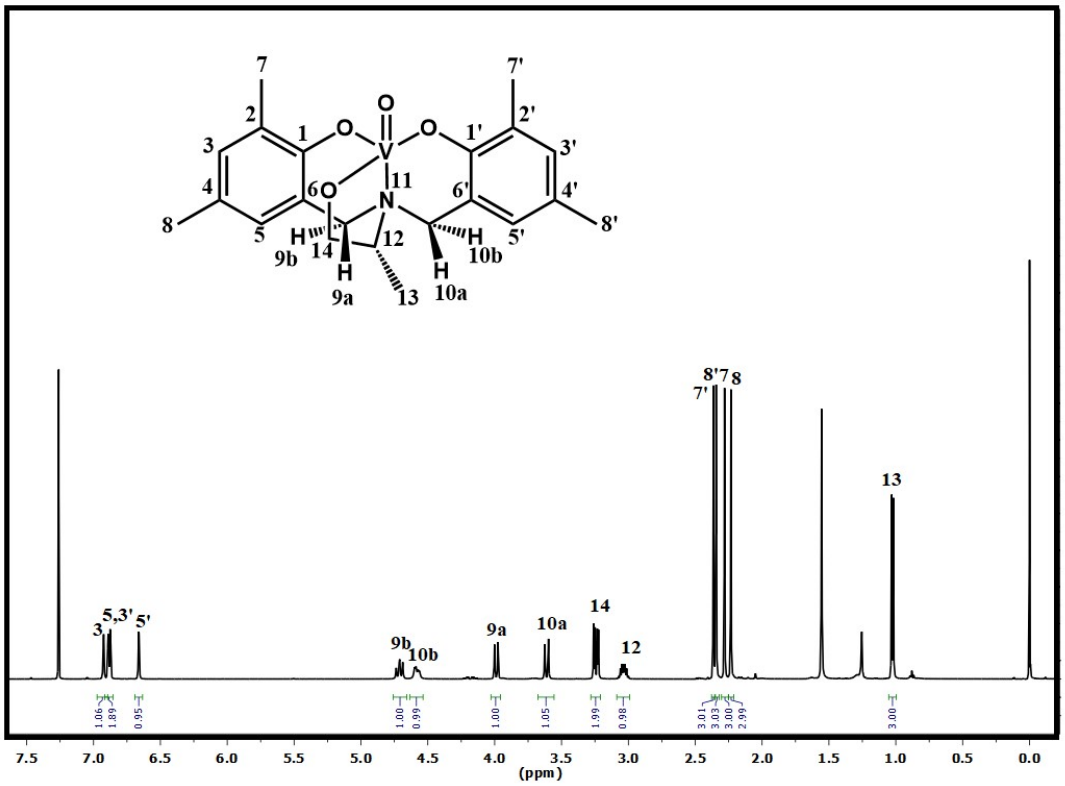

Fig. S13. ^{1}H NMR spectrum of 1 in $CDCl_3$.

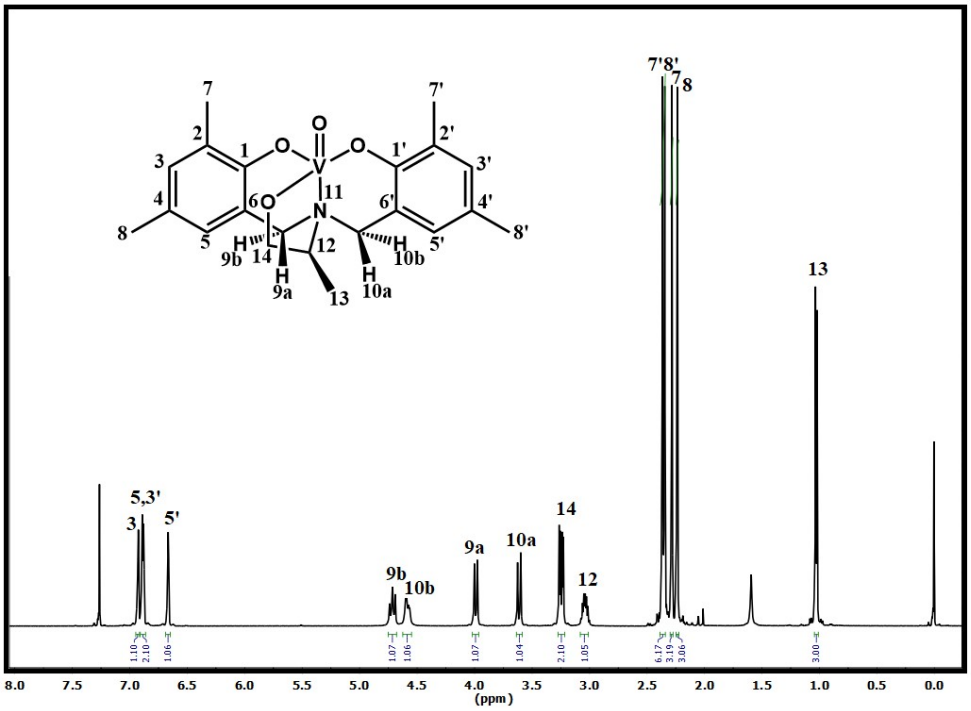

Fig. S14. ^{1}H NMR spectrum of 2 in $CDCl_3$.

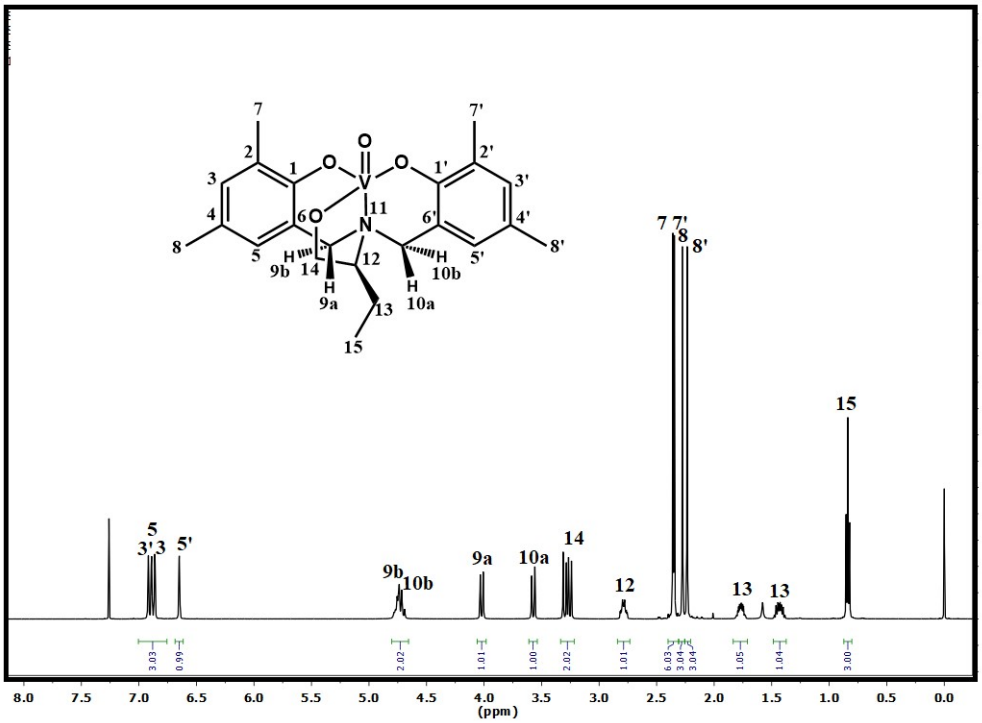

Fig. S15. ^{1}H NMR spectrum of 3 in $CDCl_3$.

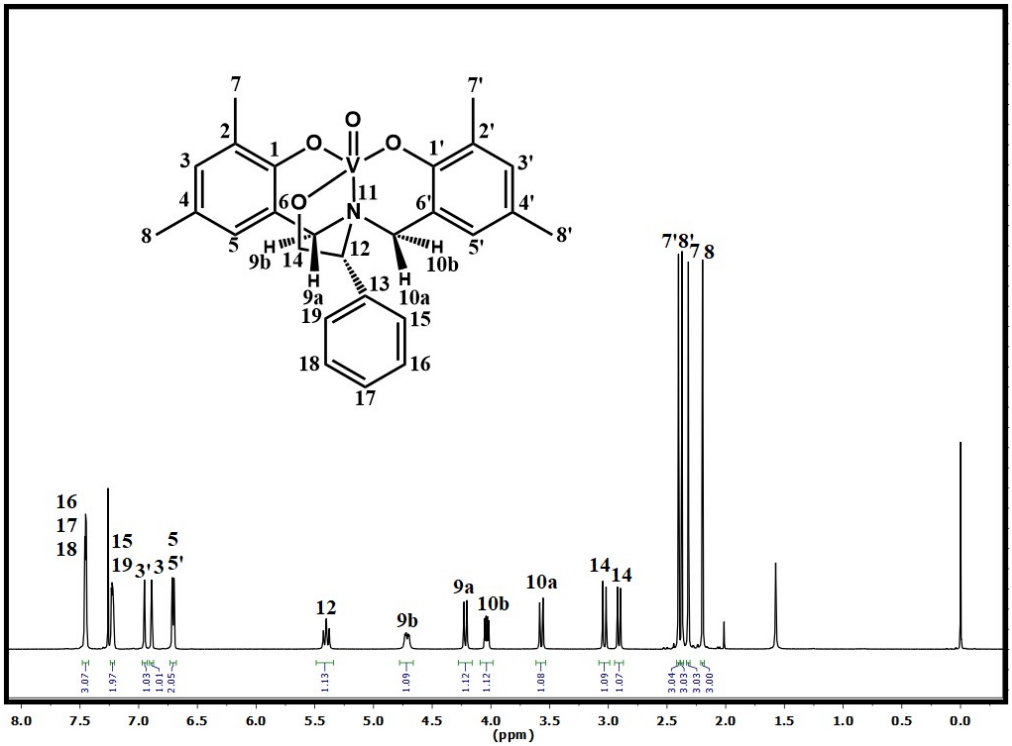

Fig. S16. ^{1}H NMR spectrum of 4 in $CDCl_3$.

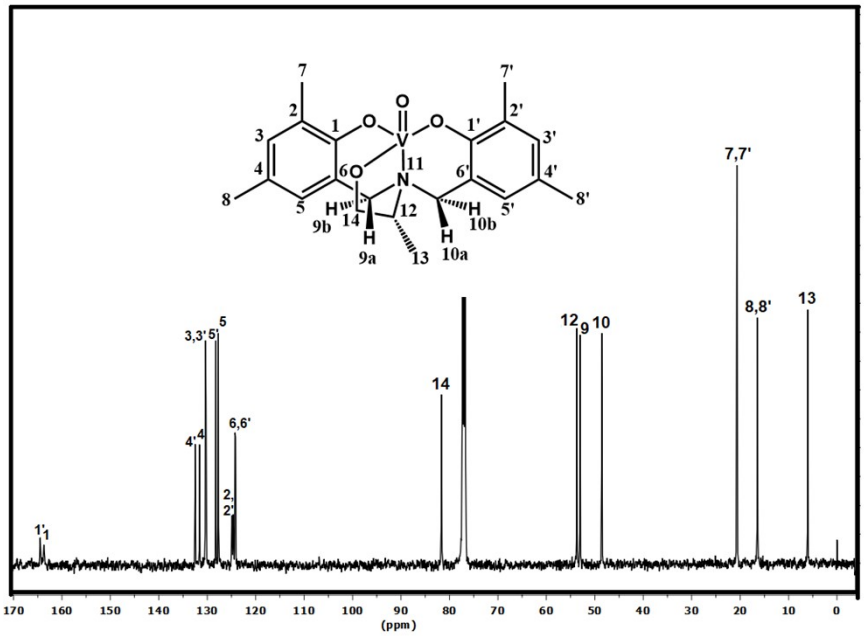

Fig. S17. ^{13}C NMR spectrum of 1 in $CDCl_3$.

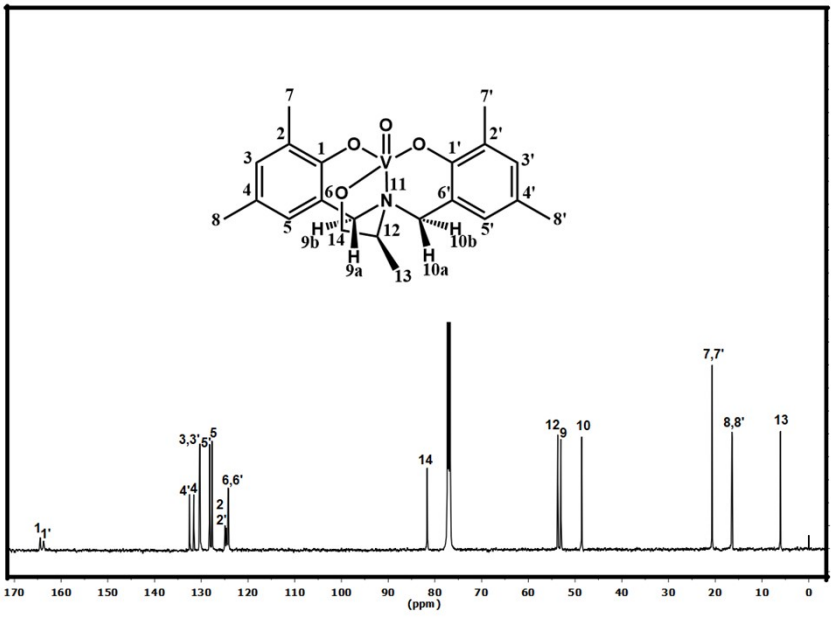

Fig. S18. ^{13}C NMR spectrum of 2 in $CDCl_3$.

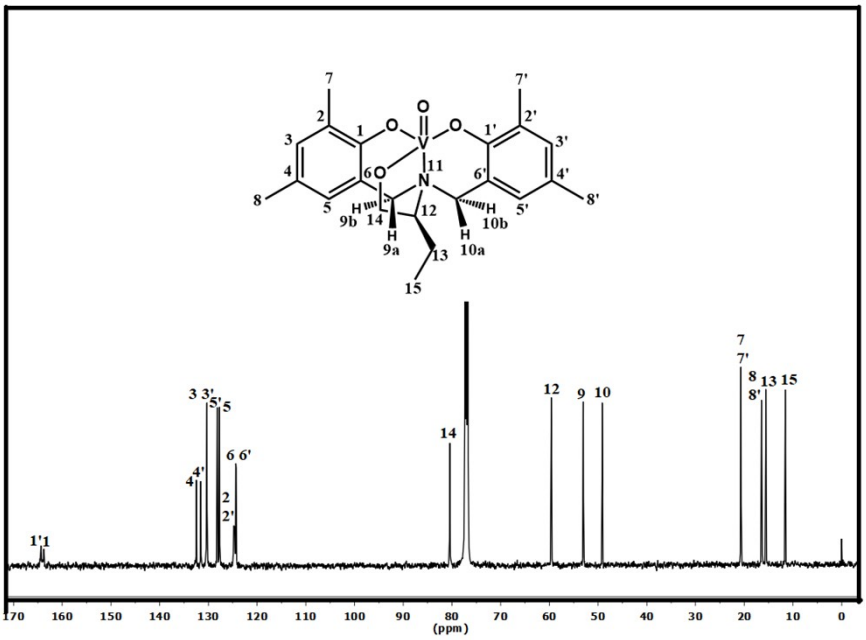

Fig. S19. ^{13}C NMR spectrum of 3 in $CDCl_3$.

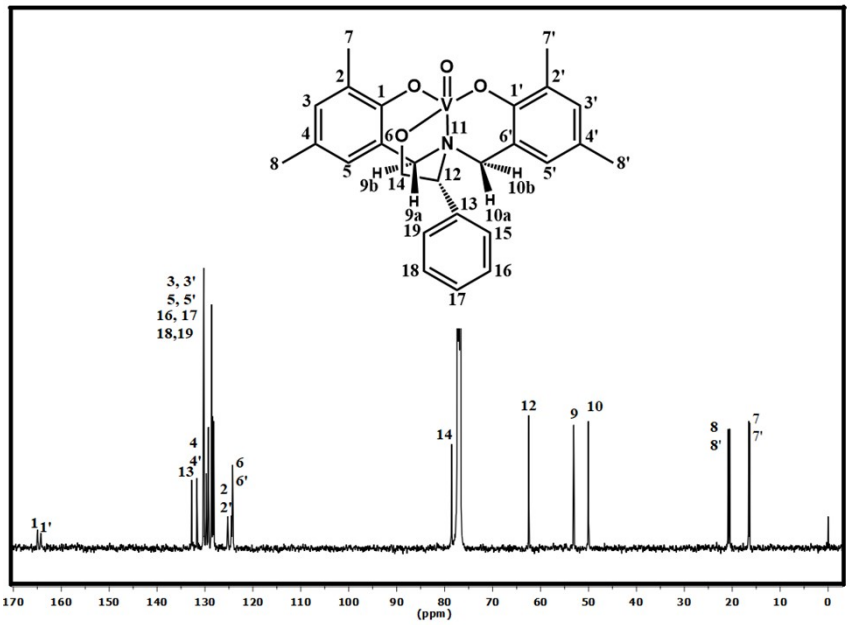

Fig. S20. ^{13}C NMR spectrum of 4 in $CDCl_3$.

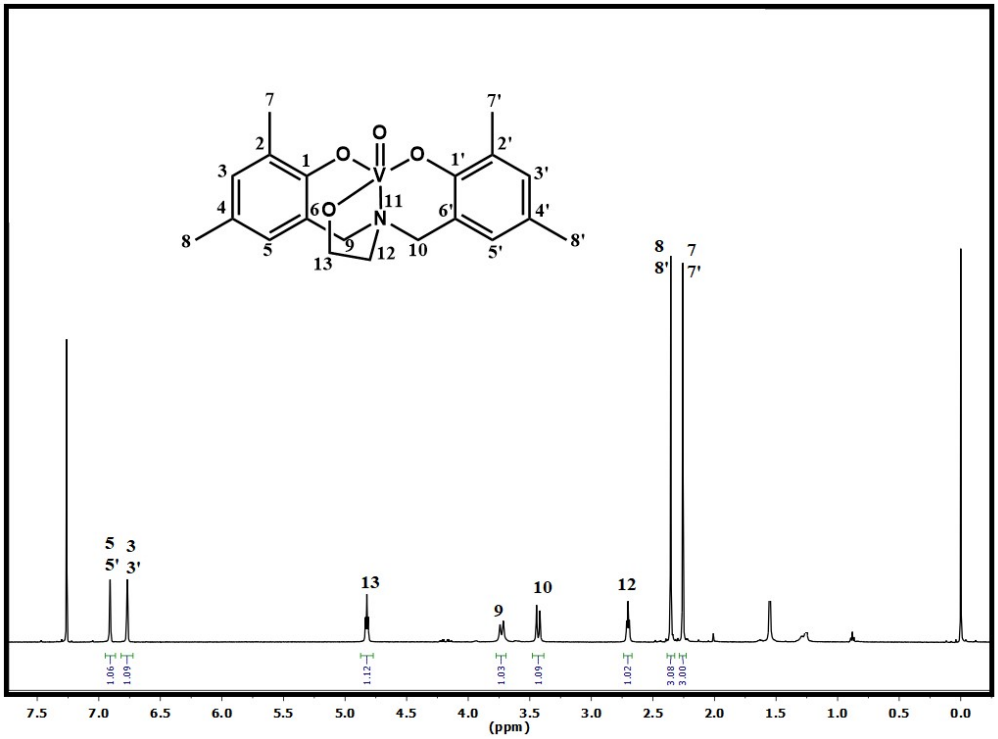

Fig. S21. ^{1}H NMR spectrum of 5 in $CDCl_3$.

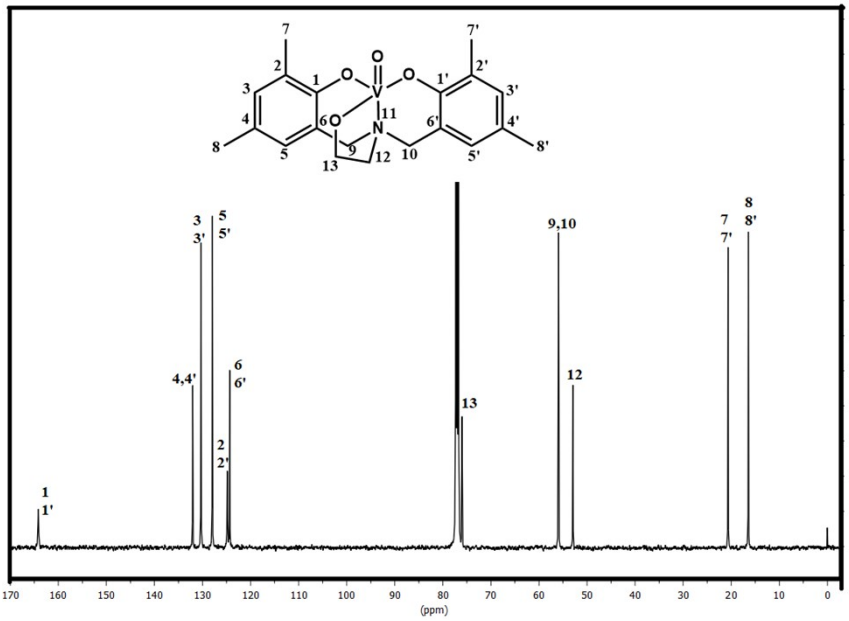

Fig. S22. ^{13}C NMR spectrum of 5 in $CDCl_3$.

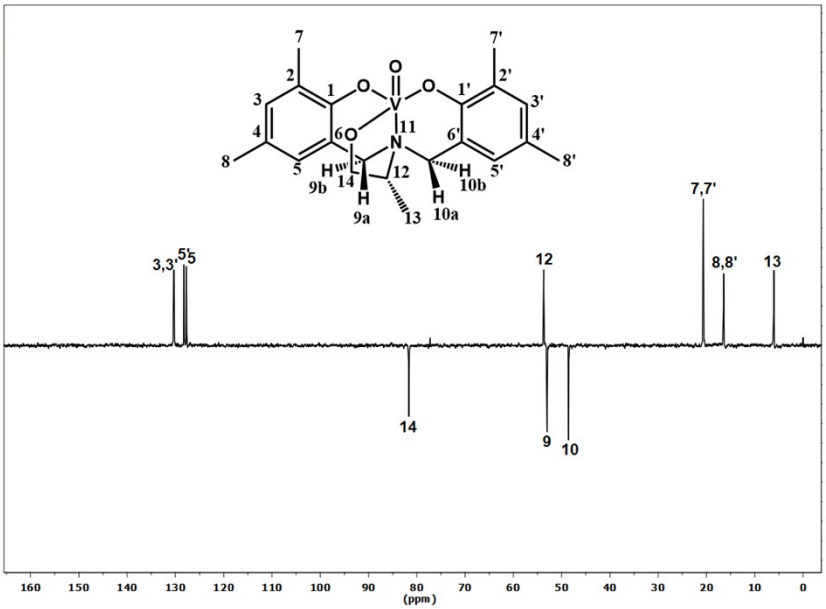

Fig. S23. ^{13}C DEPT-135 NMR spectrum of 1 in $CDCl_3$.

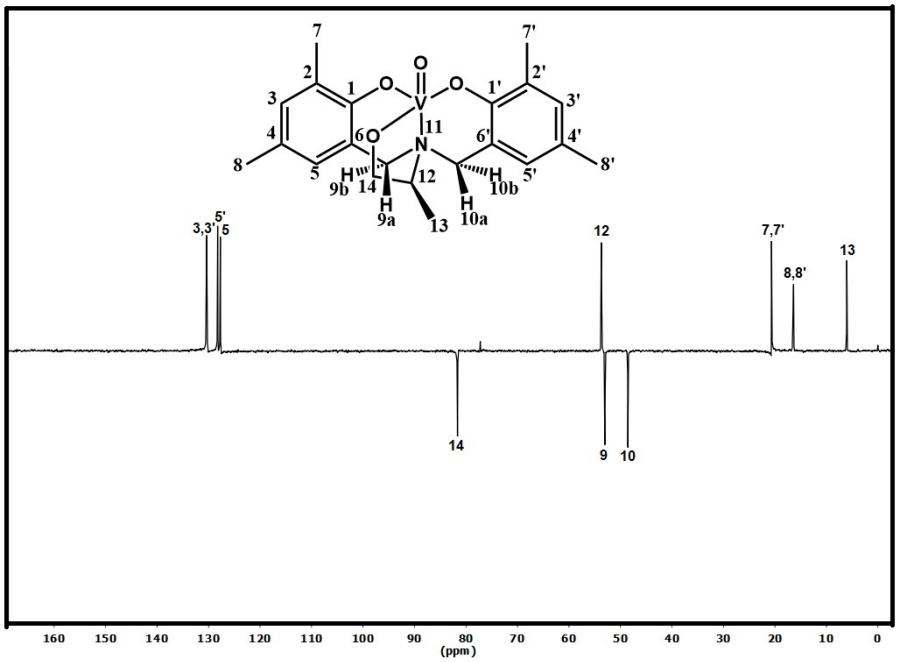

Fig. S24. ^{13}C DEPT-135 NMR spectrum of 2 in $CDCl_3$.

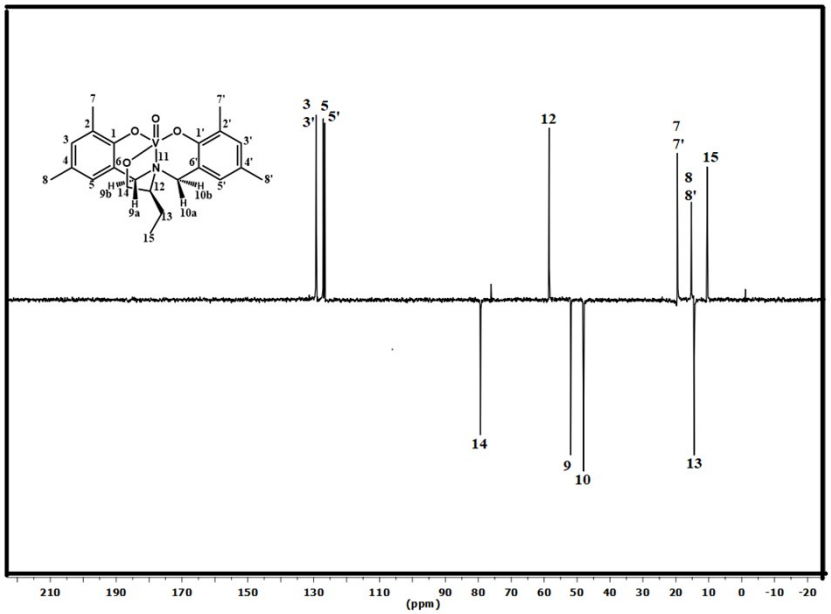

Fig. S25. ^{13}C DEPT-135 NMR of 3 in $CDCl_3$.

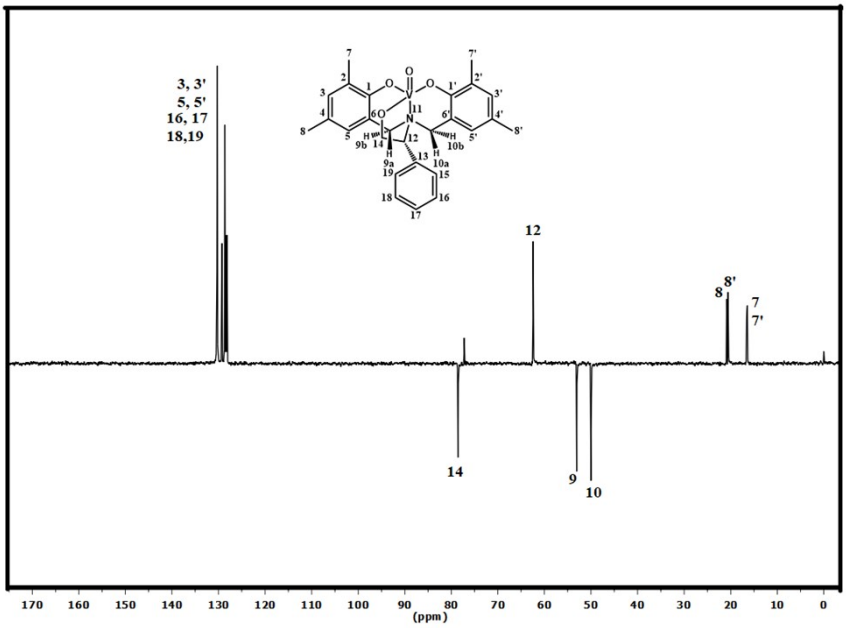

Fig. S26. ^{13}C DEPT-135 NMR of 4 in $CDCl_3$.

Fig. S27. ^{13}C DEPT-135 NMR of 5 in $CDCl_3$.

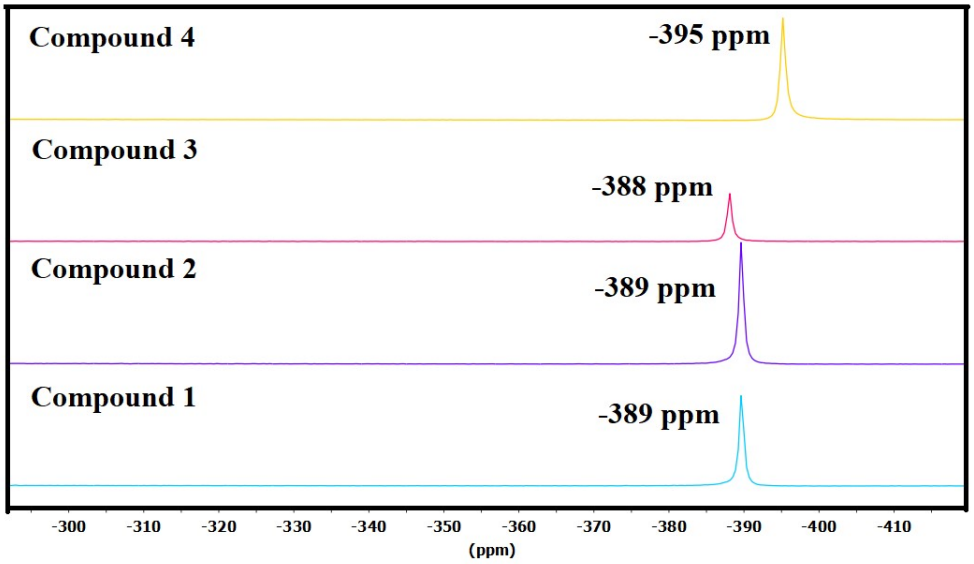

Fig. S28. ^{51}V NMR spectra of 1-4 in $CDCl_3$.

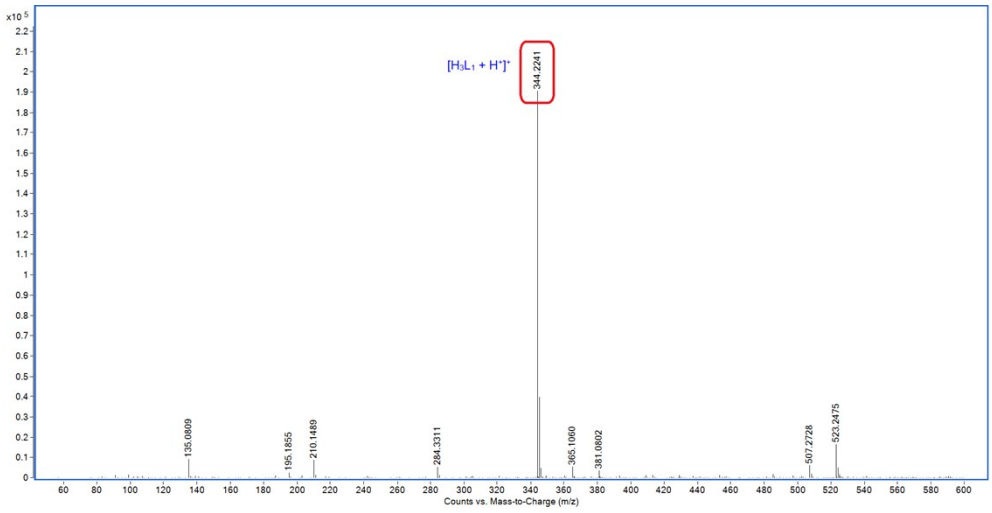

Fig. S29. ESI-MS spectrum of H_3L_1.

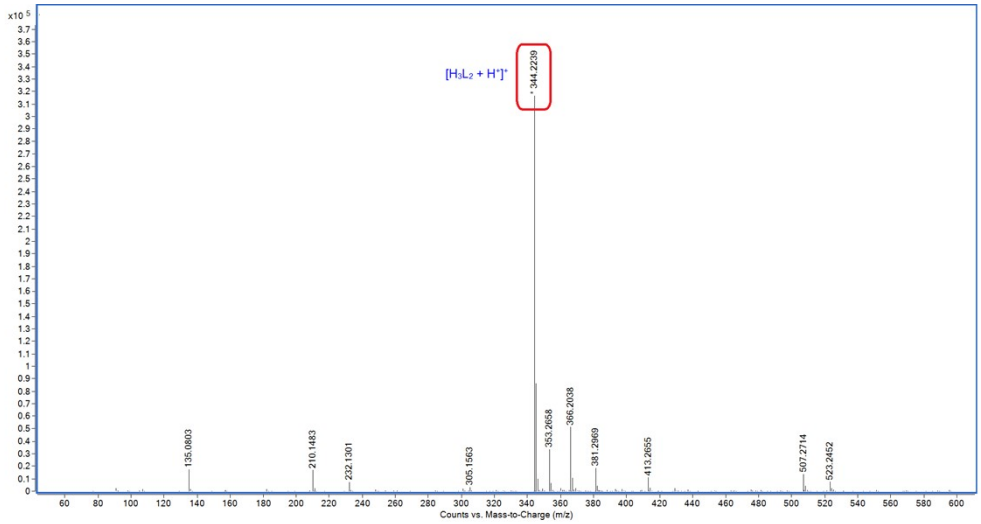

Fig. S30. ESI-MS spectrum of H_3L_2.

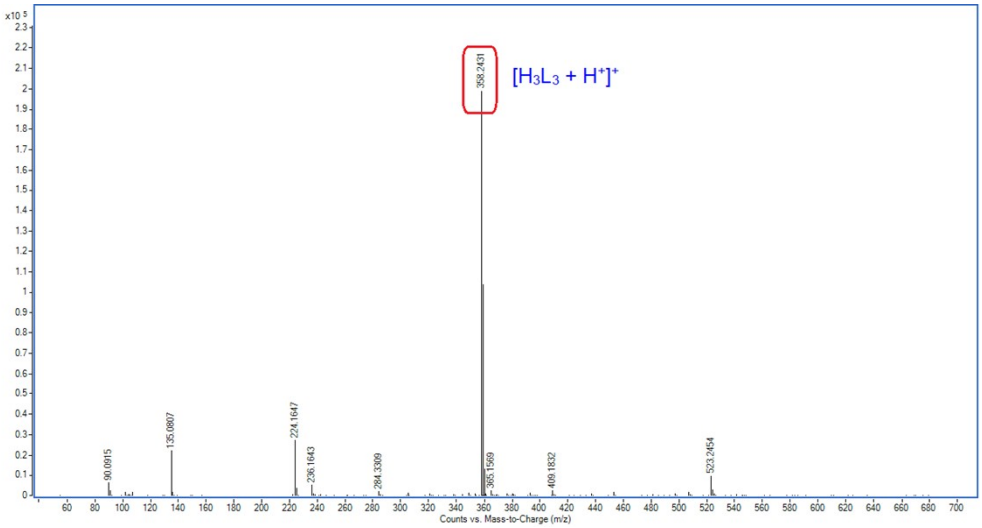

Fig. S31. ESI-MS spectrum of H_3L_3.

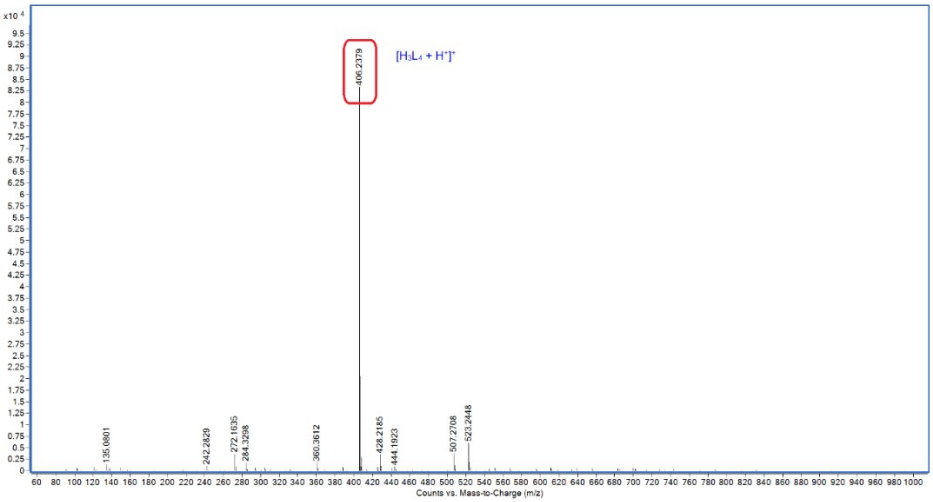

Fig. S32. ESI-MS spectrum of H_3L_4.

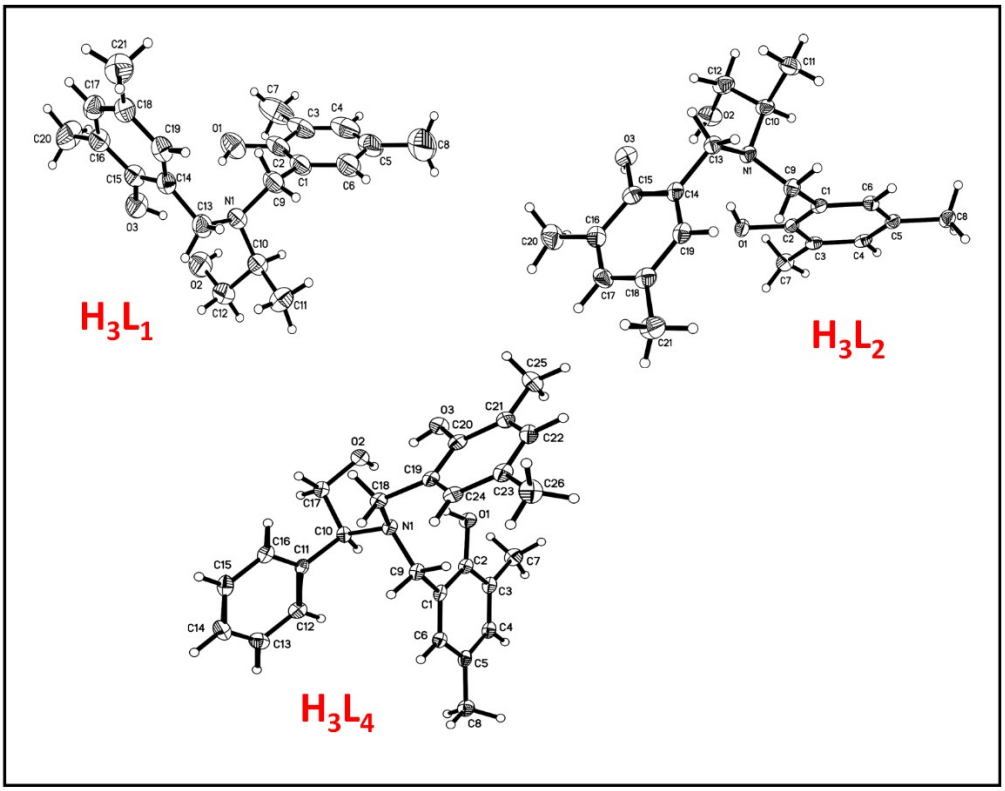

Fig. S33. ORTEP view and atom numbering scheme of H_3L_1, H_3L_2, and H_3L_4. The ellipsoids represent a 30 % probability for H_3L_1 and 50 % probability for H_3L_2 and H_3L_4, respectively. Solvent molecules are not shown for clarity.

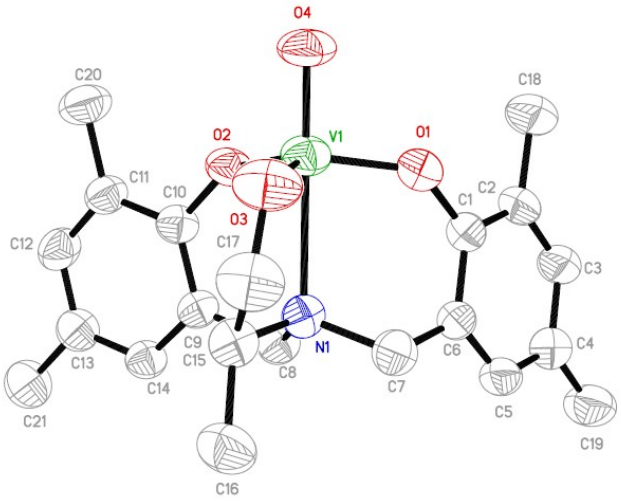

Fig. S34. ORTEP view and atom numbering scheme of compound 1. The ellipsoids represent a 50 % probability level displacement. Hydrogen atoms are not shown for clarity.

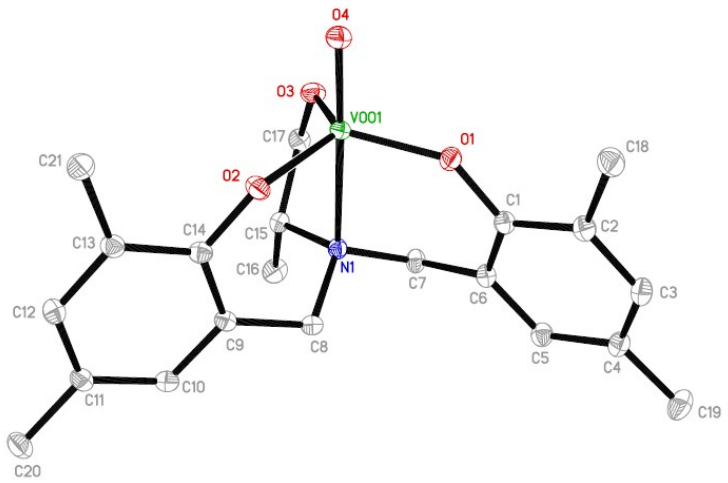

Fig. S35. ORTEP view and atom numbering scheme of compound 2. The ellipsoids represent a 50 % probability level displacement. Hydrogen atoms and solvent molecule are not shown for clarity.

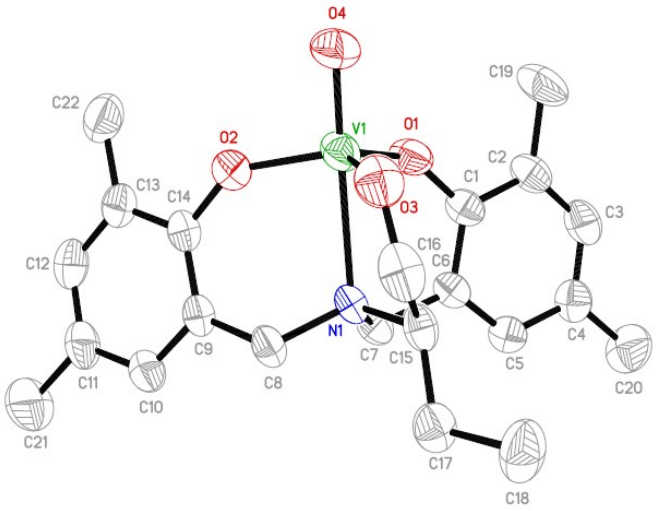

Fig. S36. ORTEP view and atom numbering scheme of compound 3. The ellipsoids represent a 50 % probability level displacement. Hydrogen atoms are not shown for clarity.

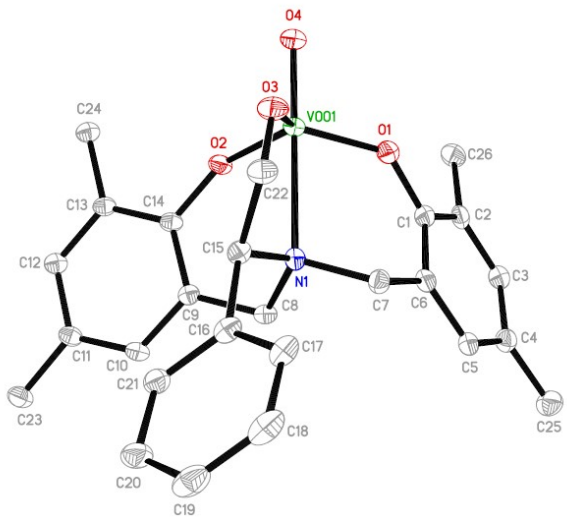

Fig. S37. ORTEP view and atom numbering scheme of compound 4. The ellipsoids represent a 50 % probability level displacement. Hydrogen atoms and solvent molecule are not shown for clarity.

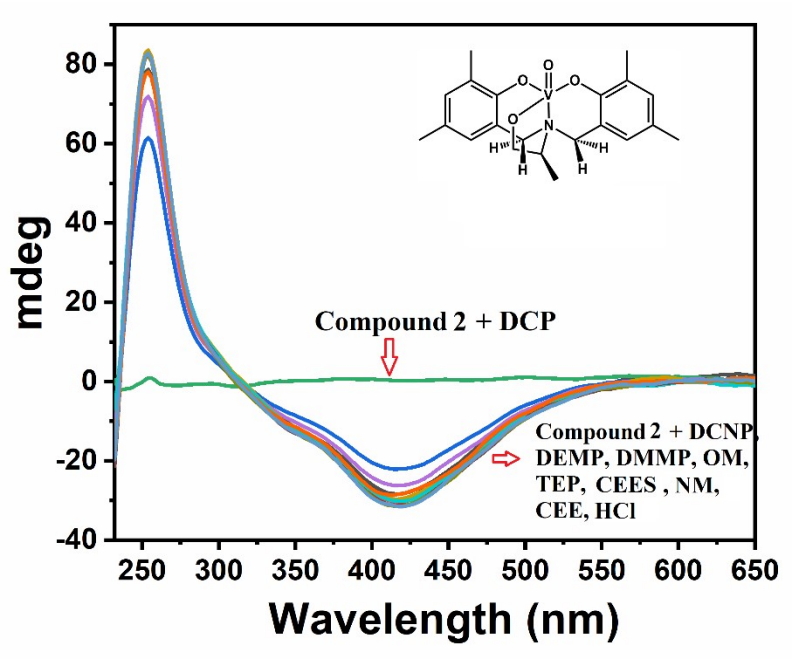

Fig. S38. CD spectra of 2 (50 µM) towards different CWAs in acetonitrile solution.

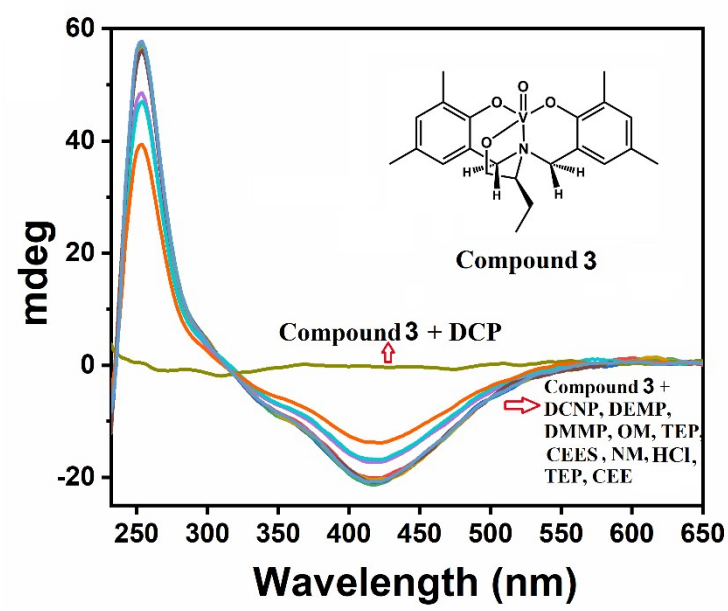

Fig. S39. CD spectra of 3 (50 µM) towards different CWAs in acetonitrile solution.

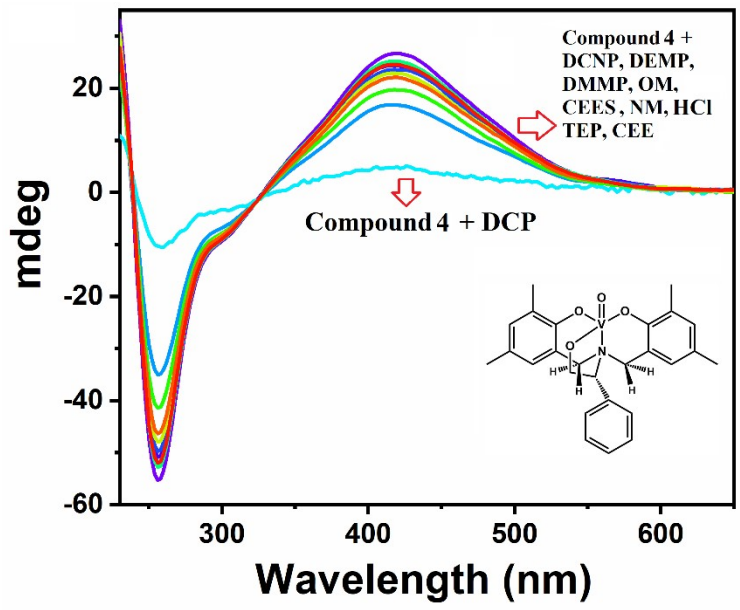

Fig. S40. CD spectra of 4 (50 µM) towards different CWAs in acetonitrile solution.

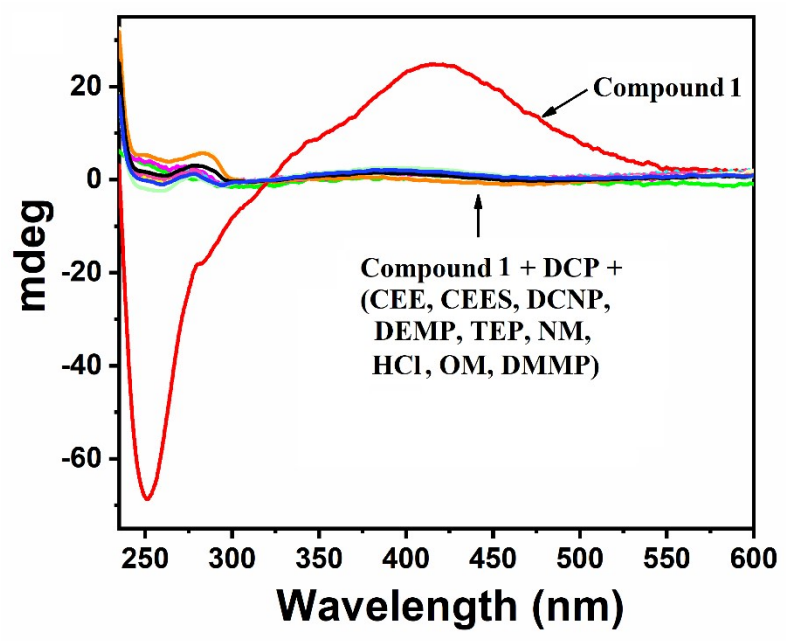

Fig. 41. CD based interference study showing selective CD response of 1 (50 µM) with DCP (2 mM) in presence of equivalent amount of other competing NAs in acetonitrile solvent.

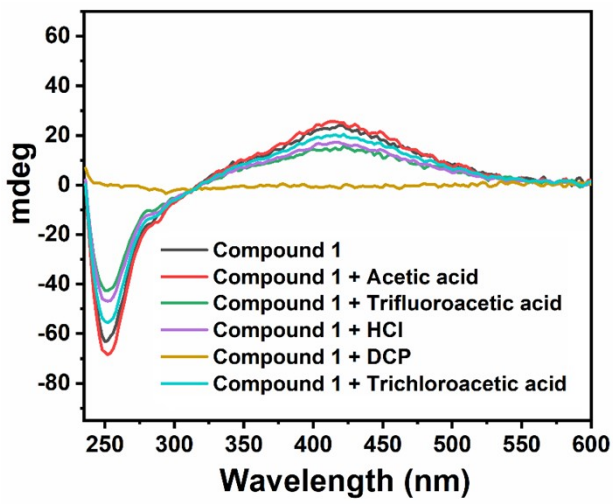

Fig. S42. CD spectra of 1 (50 µM) towards 20 equivalents of different potential interferents in acetonitrile solution.

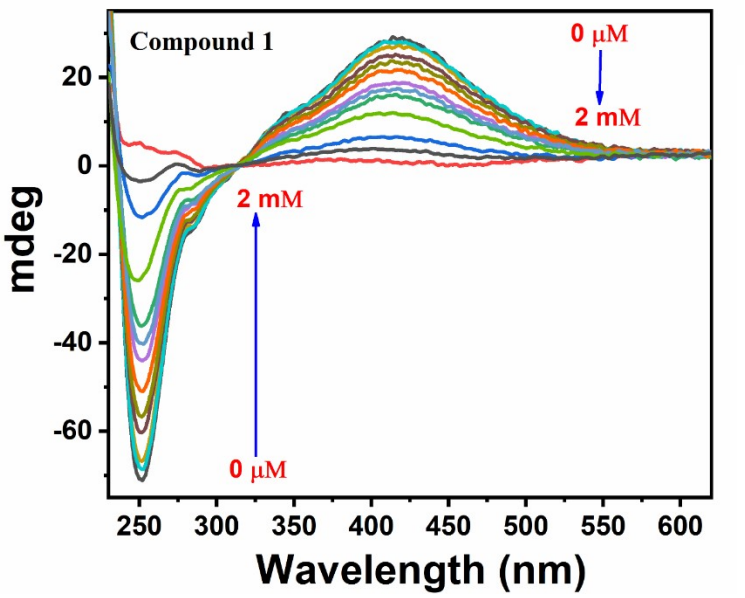

Fig. S43. CD based titration profile of 1 with increasing contents of DCP in acetonitrile.

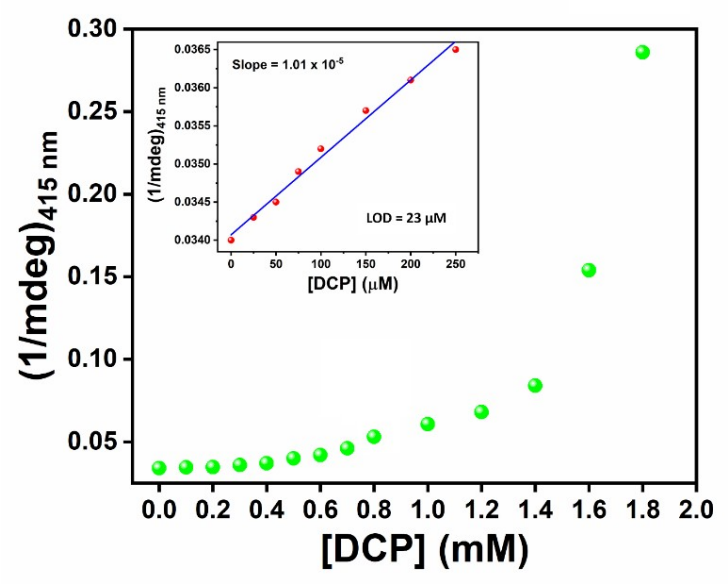

Fig. S44. CD based titration profile of 1 with increasing concentration of DCP. Inset: Limit of detection (LOD) determination plot from the titration data of 1 with increasing concentrations of DCP in acetonitrile solvent.

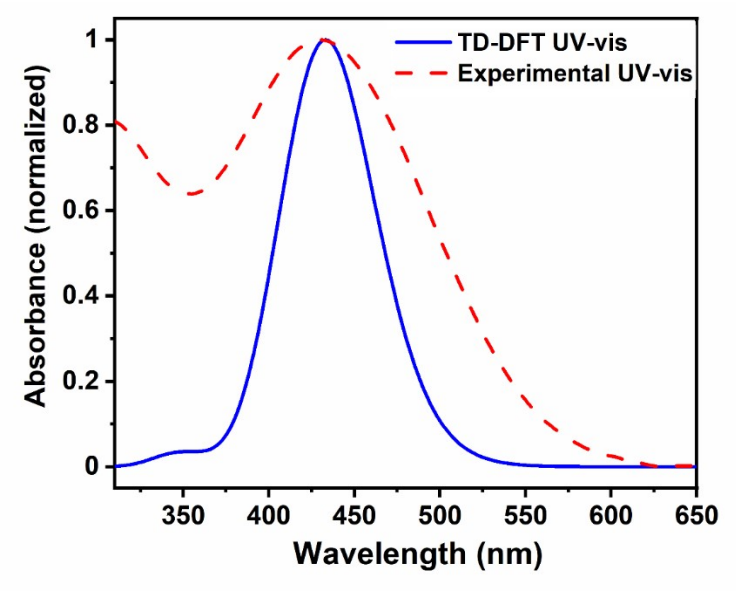

Fig. S45. Comparison of the TD-DFT based UV/vis data along with experimentally observed spectrum of 1.

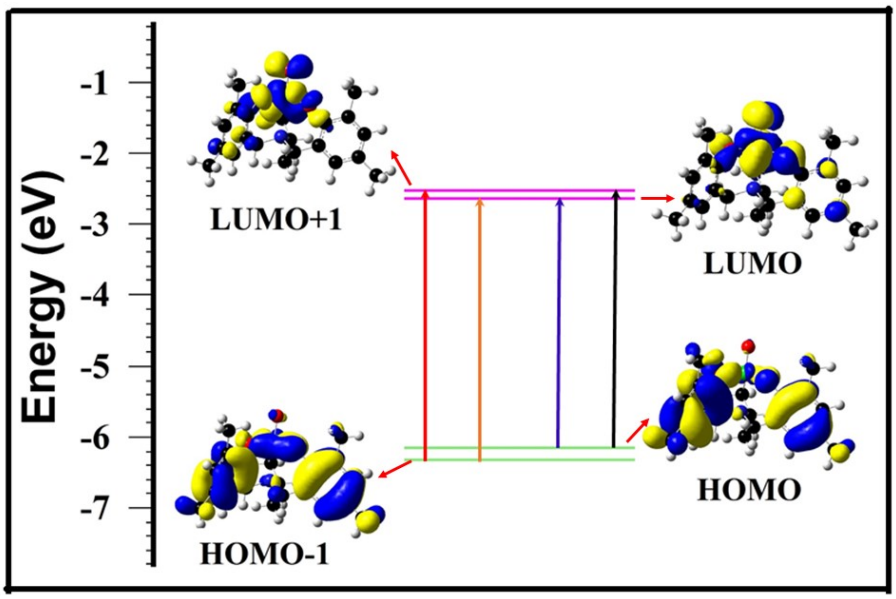

Fig. S46. TD-DFT derived energy (eV) and contour diagram (0.04 au) of the selected frontier molecular orbitals of 1 in acetonitrile. The arrows show major transitions. The major transitions can be assigned as ligand-to-metal-charge-transfer (LMCT) and ligand-to-ligand-charge-transfer (LLCT). Colour code: blue (positive values) and yellow (negative values).

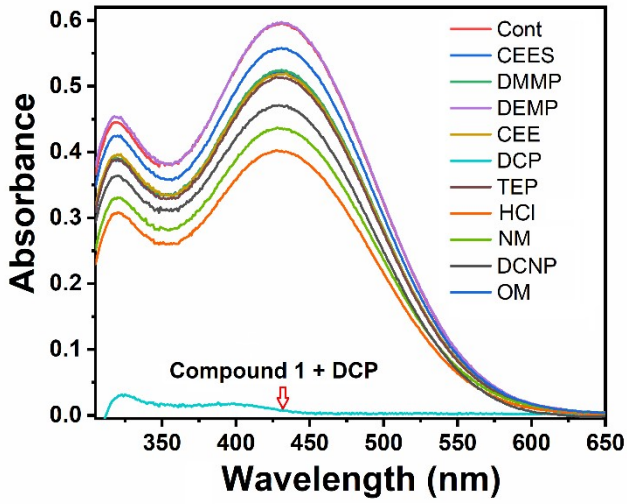

Fig. S47a. UV/vis spectra of 1 (50 µM) towards different CWAs in acetonitrile solution.

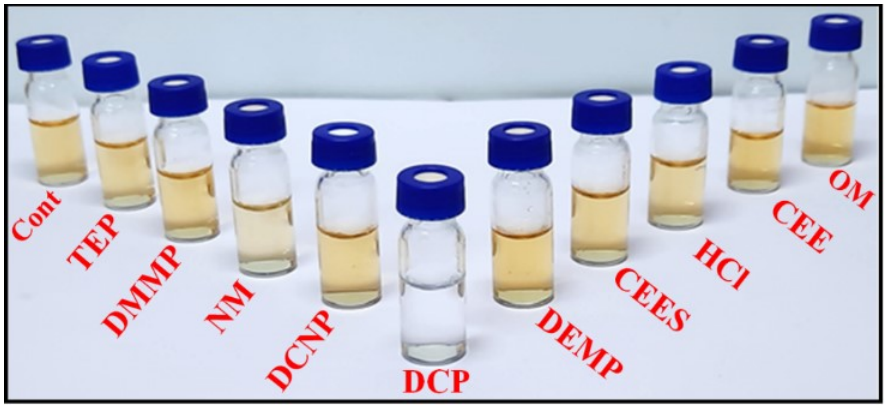

Fig. S47b. Photographs showing naked eye detection of DCP by 1 in ACN.

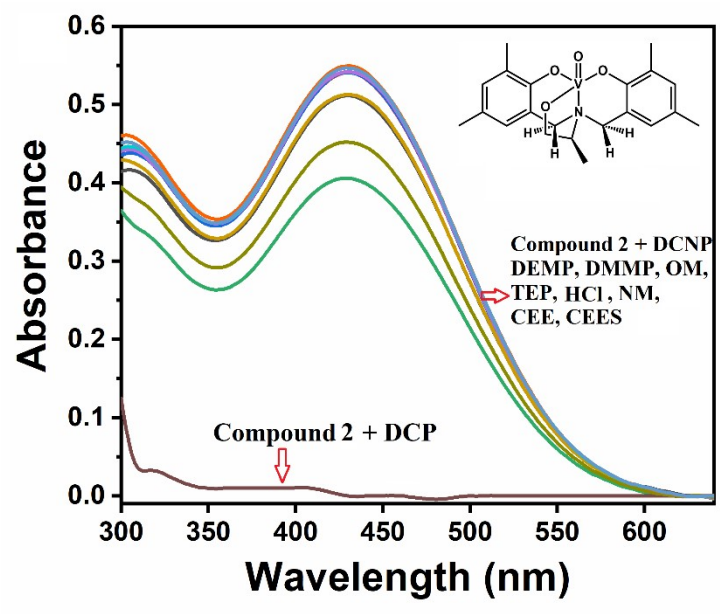

Fig. S48. UV/vis spectra of 2 (50 µM) towards different CWAs in acetonitrile solution.

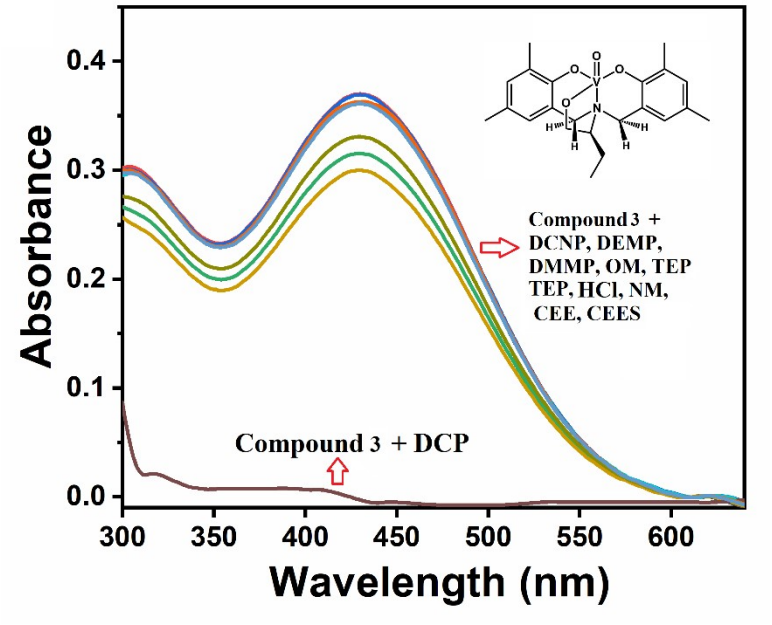

Fig. S49. UV/vis spectra of 3 (50 µM) towards different CWAs in acetonitrile solution.

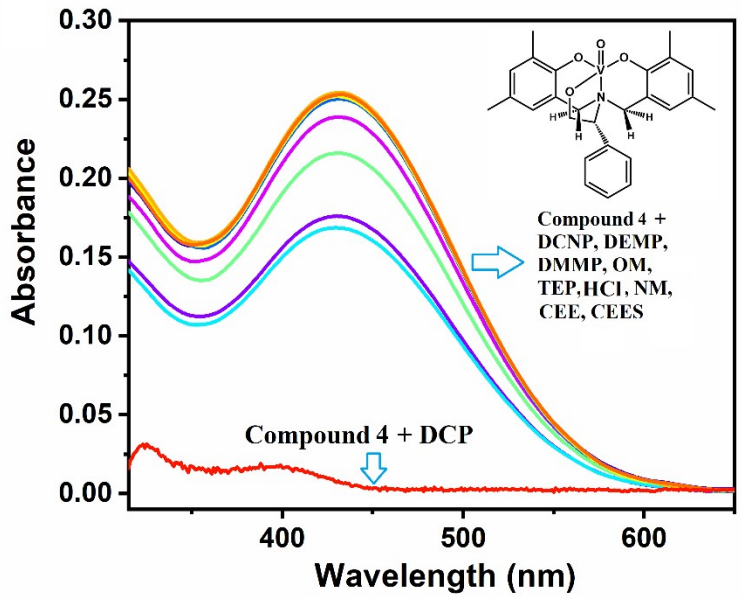

Fig. S50. UV/vis spectra of 4 (50 µM) towards different CWAs in acetonitrile solution.

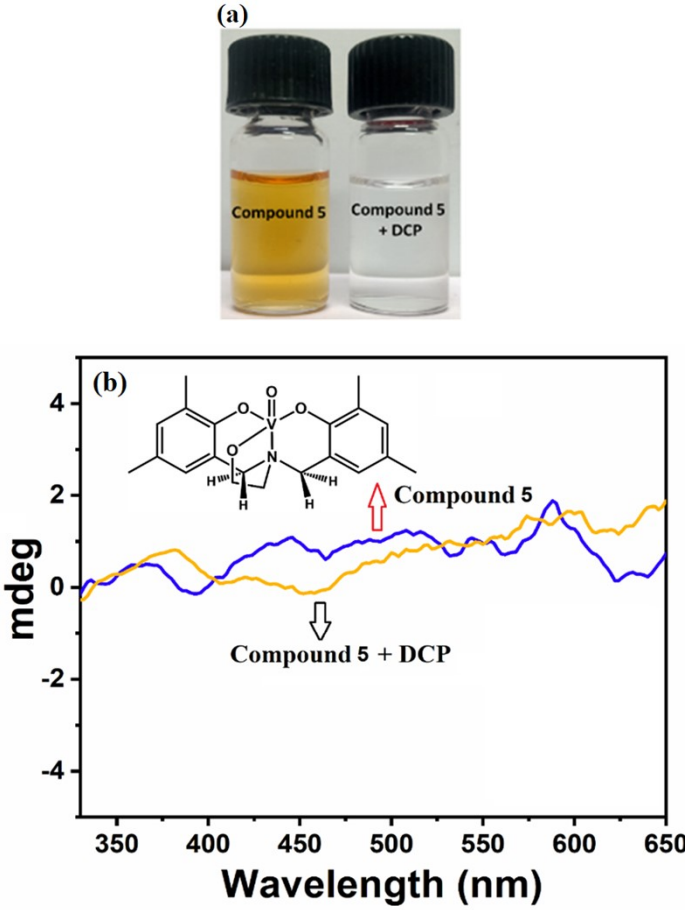

Fig. S51. (a) Photographs showing colorimetric switch of compound 5 from brown to colourless in presence of DCP. (b) CD spectra of compound 5 towards in presence and absence of DCP in acetonitrile solution.

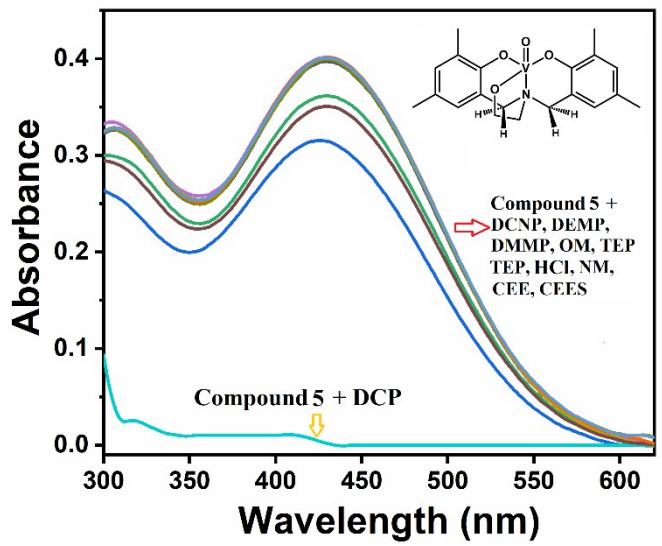

Fig. S52. UV/vis spectra of 5 towards different NAs in acetonitrile solution.

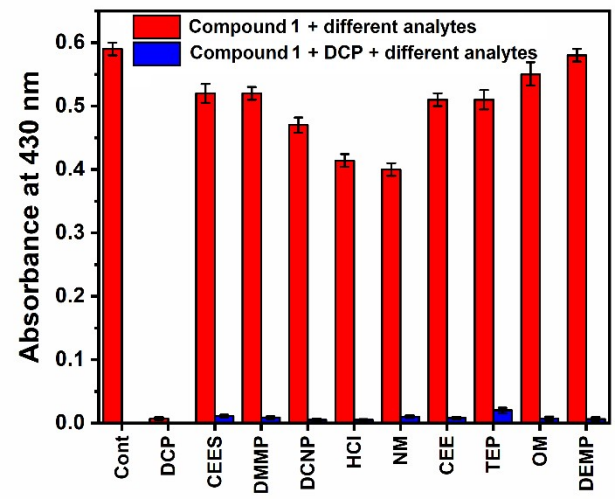

Fig. S53. Bar diagram showing selective response (UV/vis based) of 1 with DCP in presence of equivalent amount of other competing NAs in acetonitrile solvent.

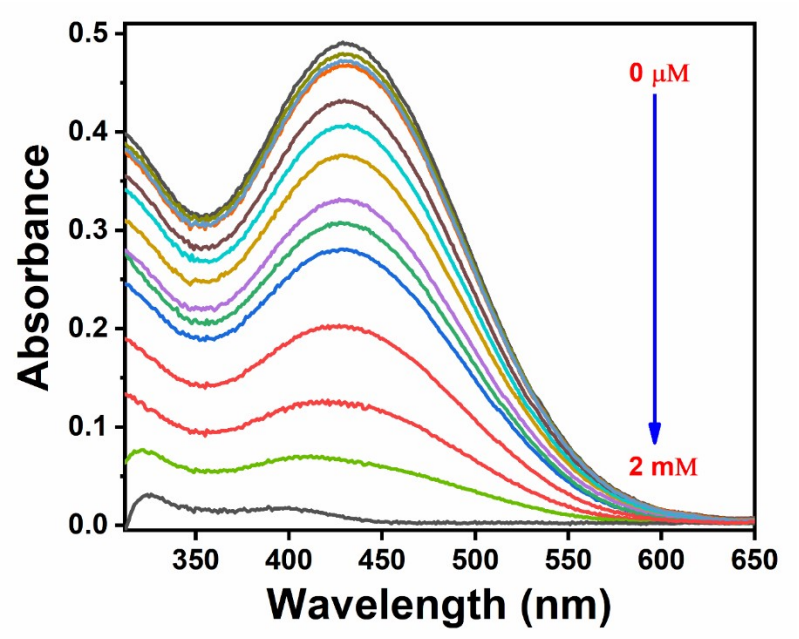

Fig. S54. UV/vis absorption titration profile of 1 with increasing contents of DCP in acetonitrile solvent.

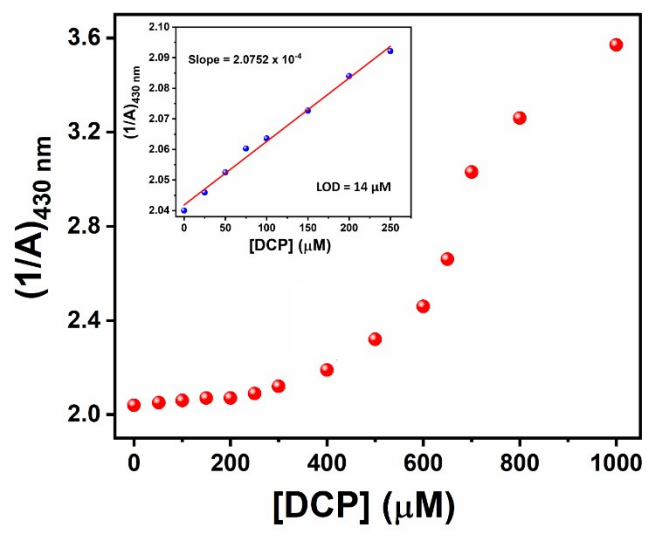

Fig. S55. UV/vis absorption profile of 1 with increasing concentration of DCP. Inset: Limit of detection (LOD) determination plot from the titration data of 1 with increasing concentrations of DCP in acetonitrile solvent.

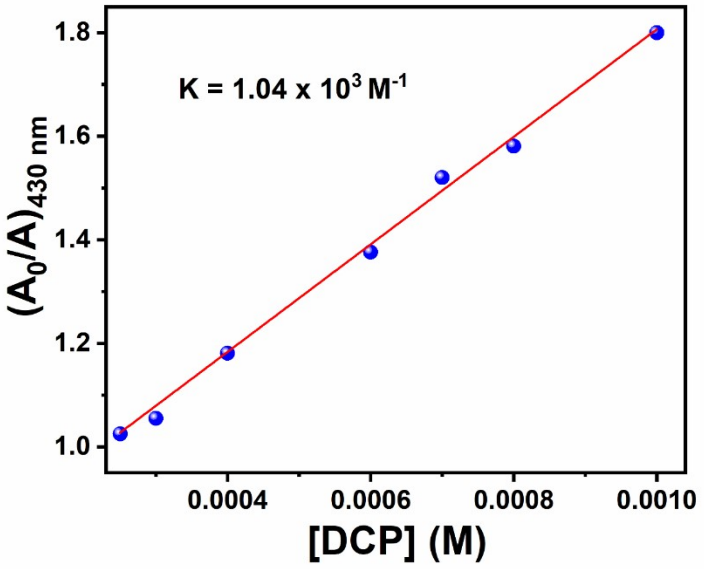

Fig. S56. Linear fittings of the UV/vis titration data points for calculating binding constant of 1 towards DCP.

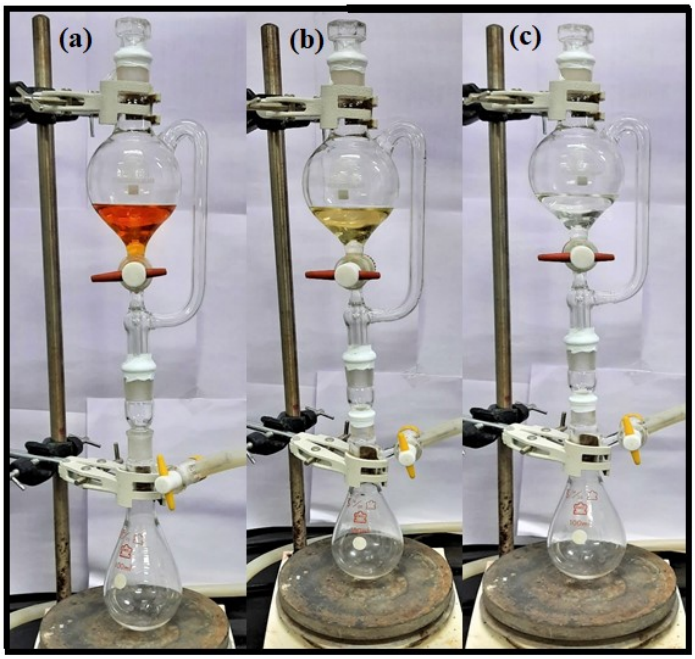

Fig. S57. Gradual chromophoric switch of the acetonitrile solution of 1 (0.1 mM) upon exposure to DCP vapour at 1 ppm.

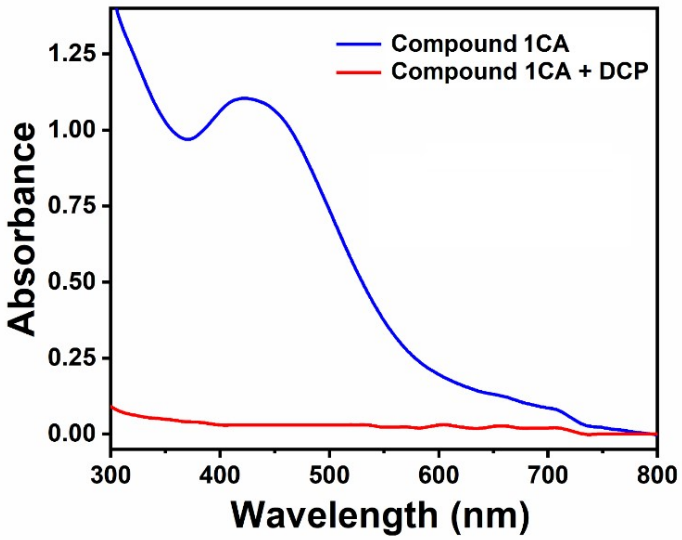

Fig. S58. UV-vis absorption profile of the chiroptode (compound 1CA) before (blue) and after (red) the exposure to DCP vapour (1 ppm).

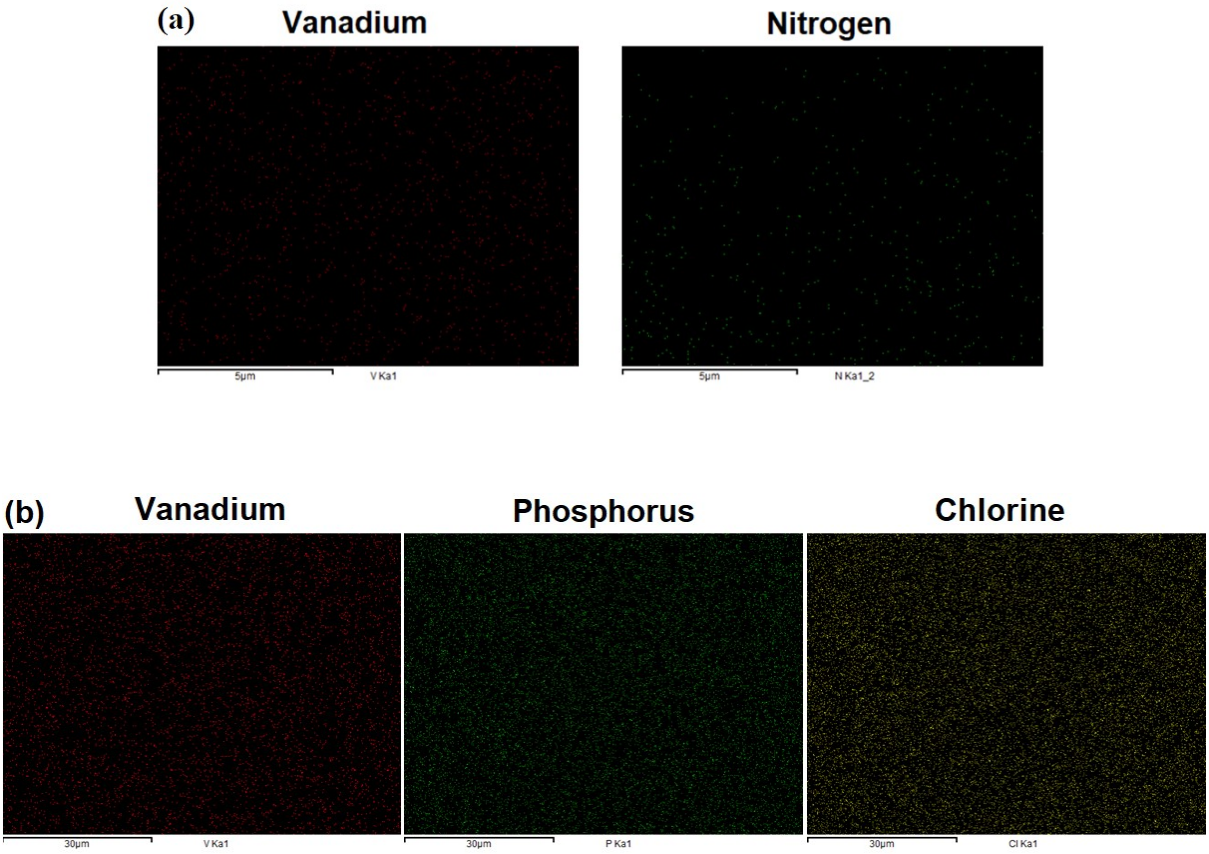

Fig. S59. SEM-EDX mapping of chiroptode (compound 1CA) before (a, upper panel) and after (b, lower panel) exposure to DCP vapour.

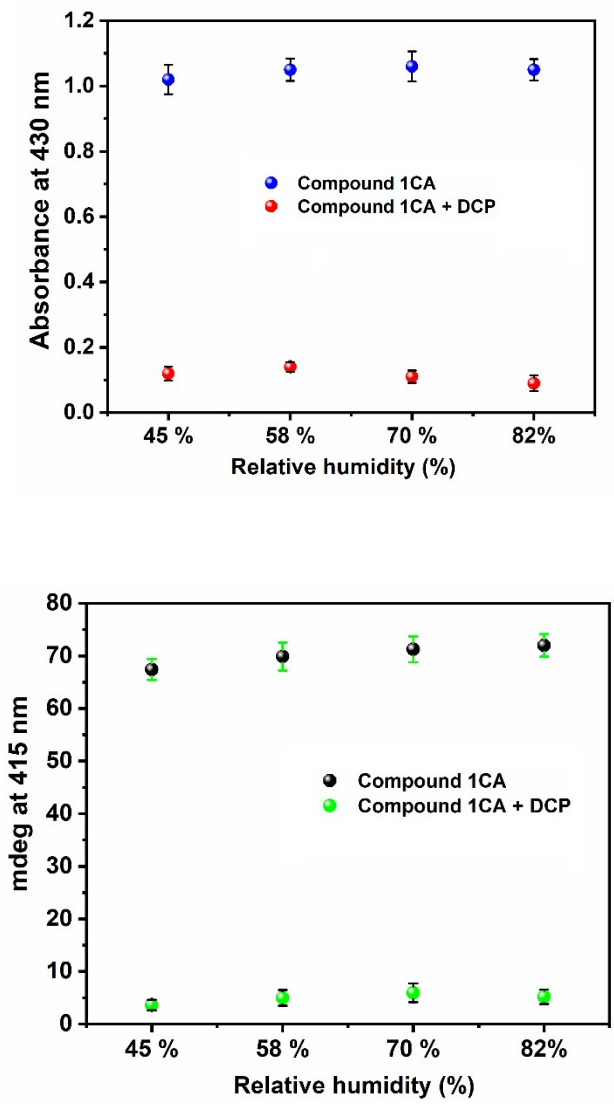

Fig. 60. Relative humidity dependent UV/vis (top panel) and CD (bottom panel) spectra of the chiroptode (compound 1CA) upon exposure to static DCP vapour (10 ppm) for 30 minutes.

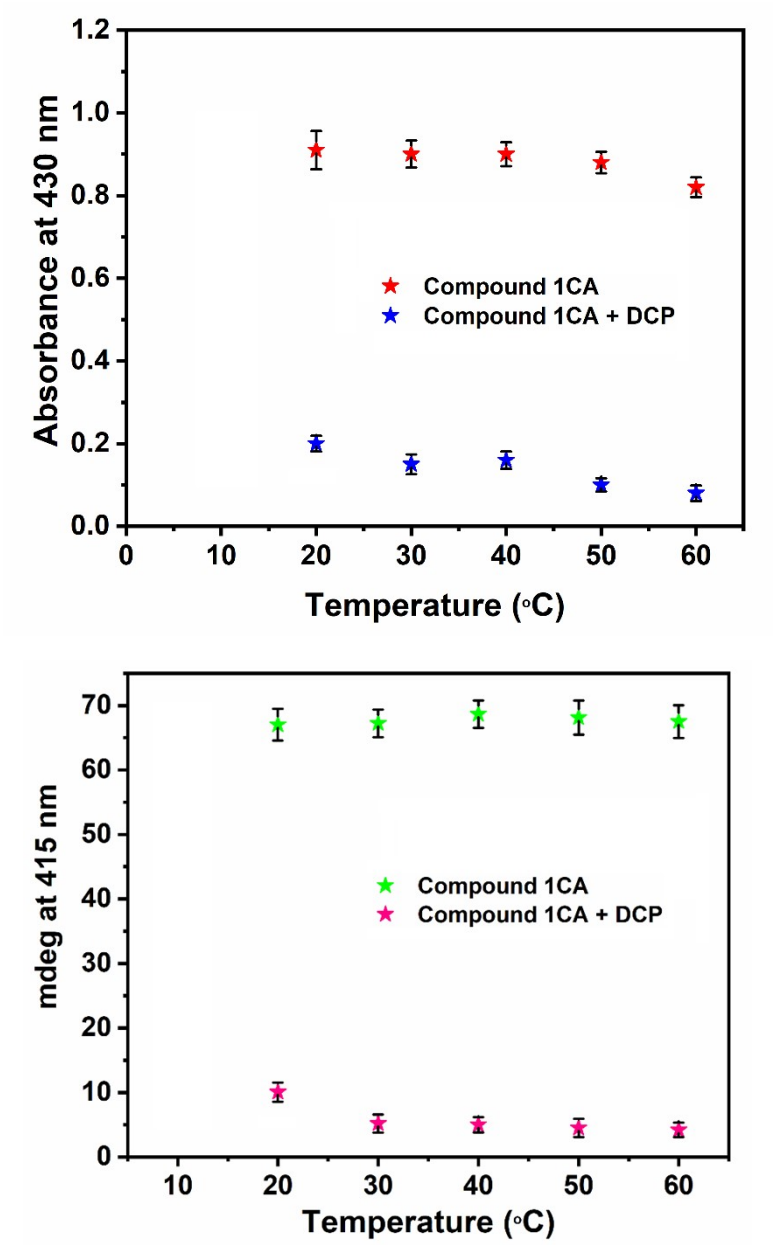

Fig. S61. Temperature dependent UV/vis (top panel) and CD (bottom panel) spectra of the chiroptode (compound 1CA) upon exposure to static DCP vapour (10 ppm) for 30 minutes.

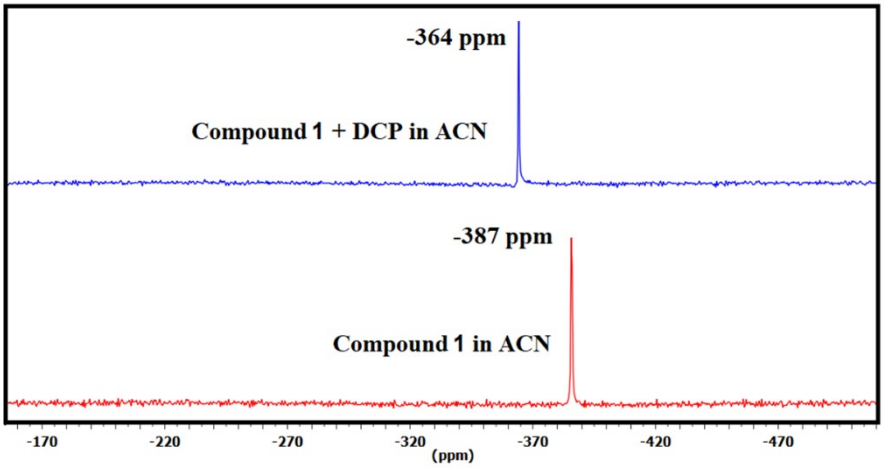

Fig. S62. Comparative ^{51}V profile of 1 recorded in ACN solvent with and without DCP.

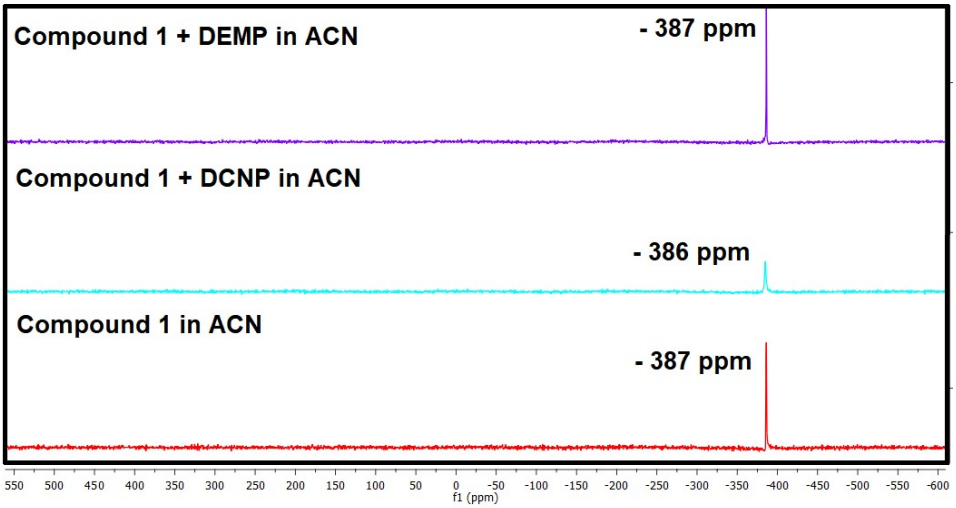

Fig. S63. Comparison of ^{51}V NMR chemical shifts of 1 in absence and presence of DCNP and DEMP, separately in acetonitrile solvent.

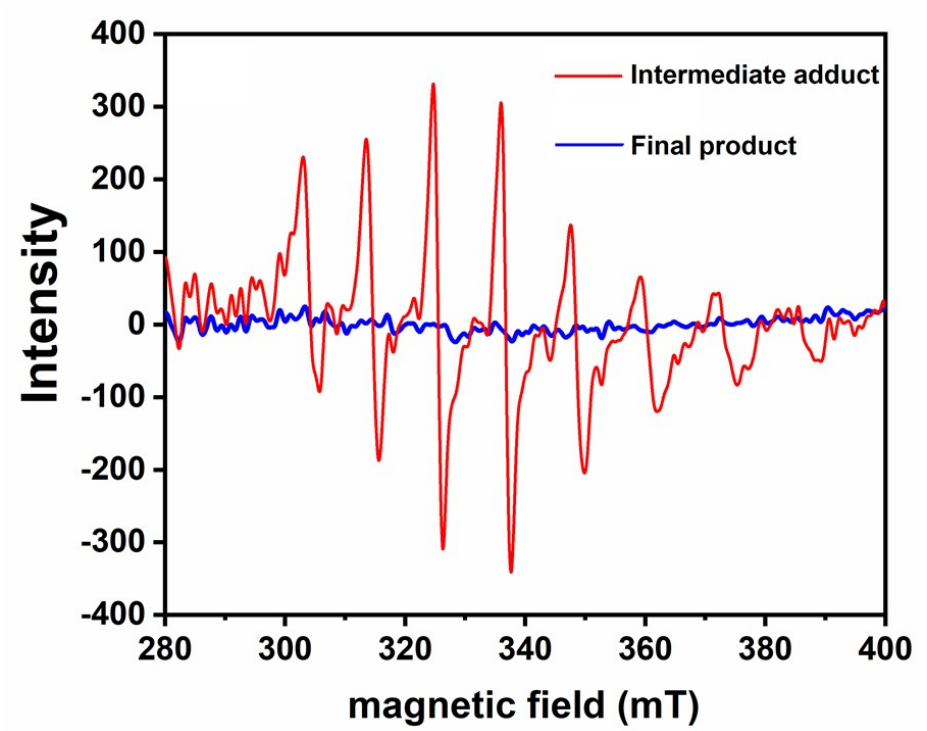

Fig. S64. EPR spectra of the intermediate vanadium(IV) species (red line) and the final adduct (blue line) after the addition of DCP. Equivalent amount of 1 and DCP were taken in ACN.

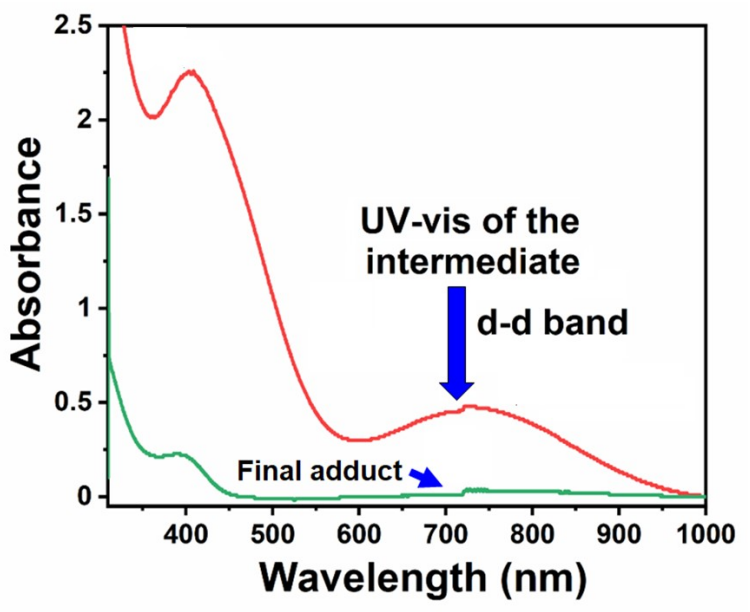

Fig. S65. UV/vis spectra of 1 in ACN solvent recorded immediately after the addition of DCP showing d-d band of the intermediate vanadium(IV) species. Equivalent amount of 1 and DCP were taken in ACN.

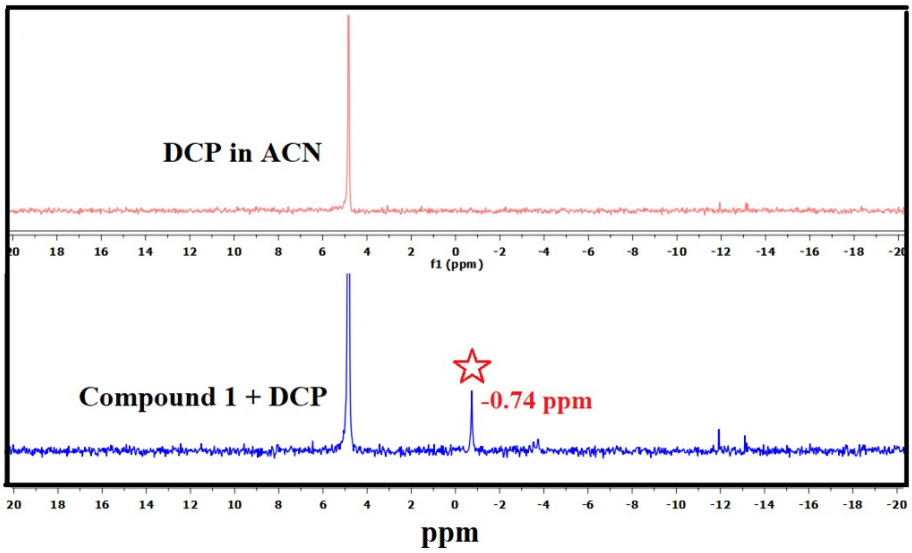

Fig. S66. Comparative ^{31}P NMR profile of DCP recorded in ACN solvent with and without 1. Asterisk indicates the formation of a new vanadium-phosphorus species.

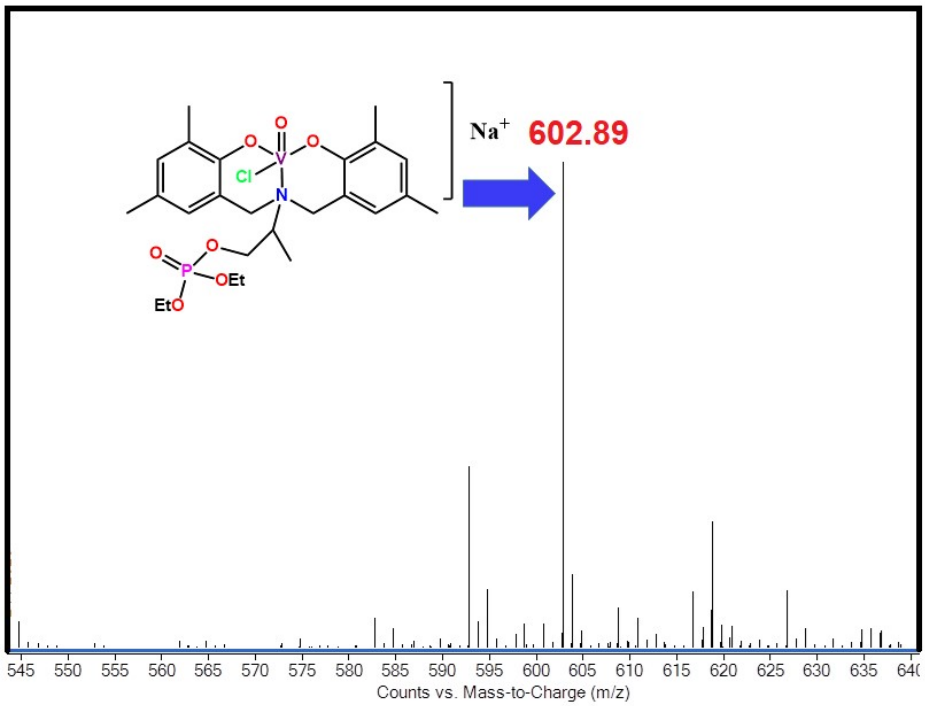

Fig. S67. ESI-MS of 1 in presence of DCP in acetonitrile solvent.

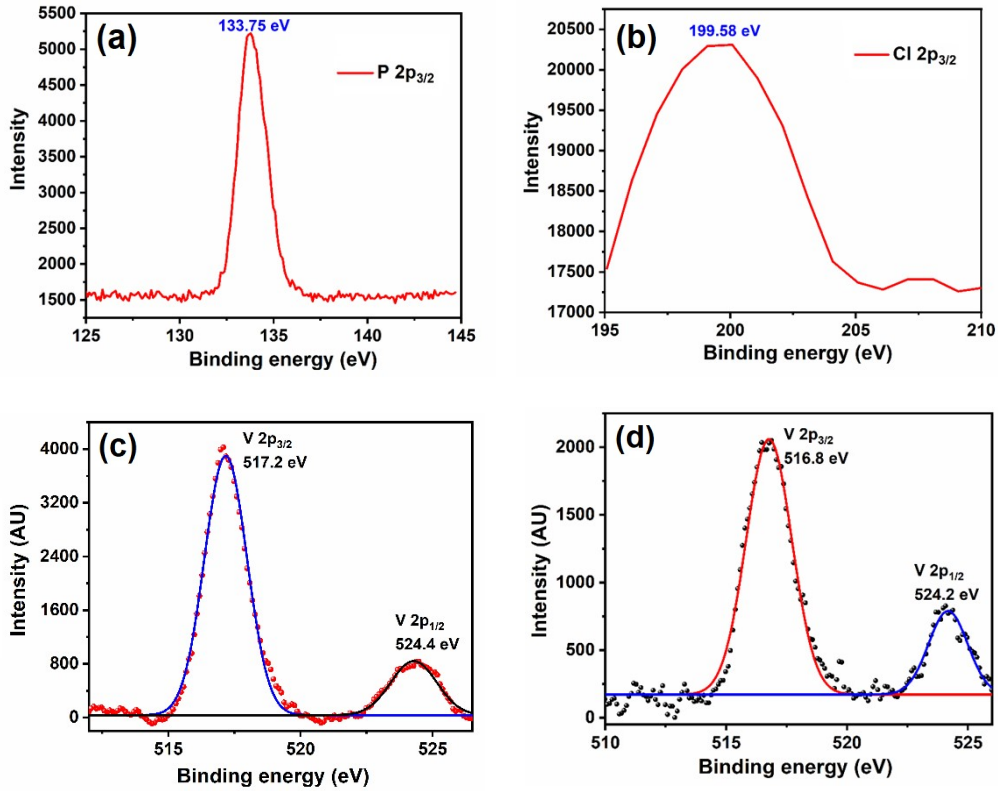

Fig. 68. XPS profiles of the 2p orbitals of phosphorus (a), chlorine (b), and vanadium (d) in the chiroptode (compound 1CA) after its exposure to the DCP vapour. Panel (c) indicates 2p orbitals of vanadium before its exposure to the DCP vapour.

Table S1. Comparative literature survey on DCP selective probes.

Sl. No	Probe	Sensing Medium	Detection technique/s	Response time	Publication
1	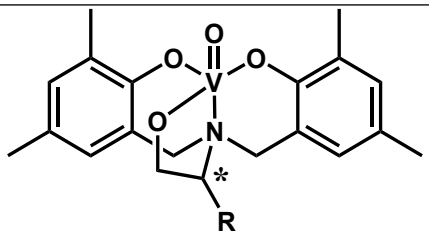	ACN	Chiroptical technique (UV/vis-CD spectroscopic response)	12 s (brown to colourless) Both vapour and liquid phases	Present work
2	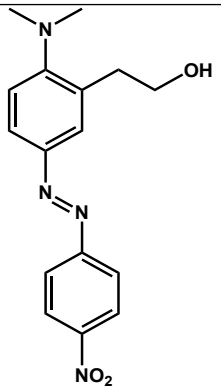	ACN	Colorimetric response	Few seconds Both vapor and liquid phases	21
3	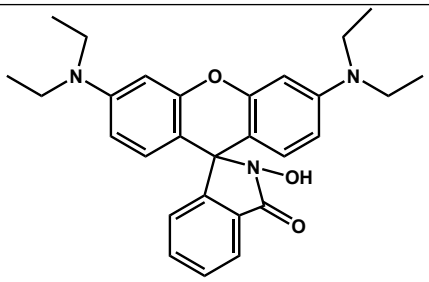	DMF containing TEA (3%, v/v)	Colorimetric and fluorometric response	20 min Both vapor and liquid phase	22
4	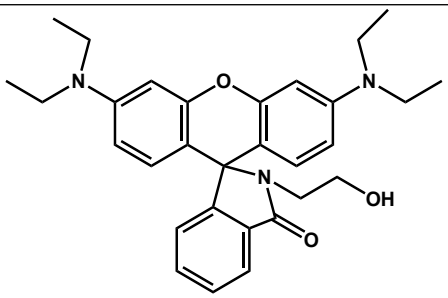	DMF containing TEA (3%, v/v)	Colorimetric and fluorometric response	5 min Liquid phase	23

5	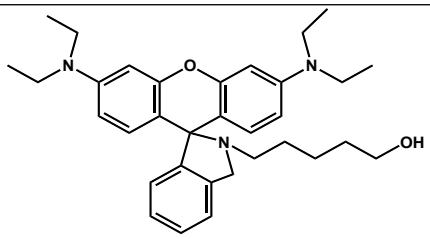	DMF	Colorimetric and fluorometric response	20 min. Liquid phase	24
6	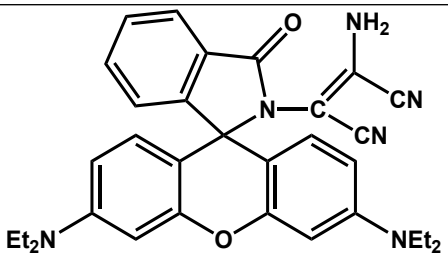	DCM containing 3 % TEA (v/v)	Colorimetric and fluorometric response	8 min. Both vapour and liquid phase	25
7	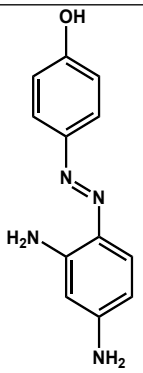	DCP ACN	Colorimetric and fluorometric response	Within 1 min. Liquid phase	26
8	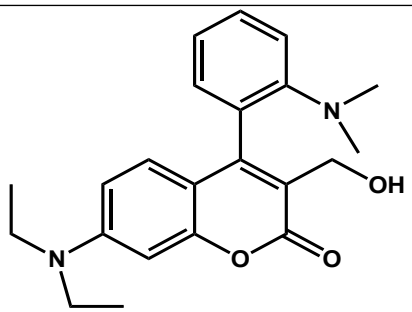	$CHCl_3$	Fluorometric response	Within 1 min. Liquid phase	27
9	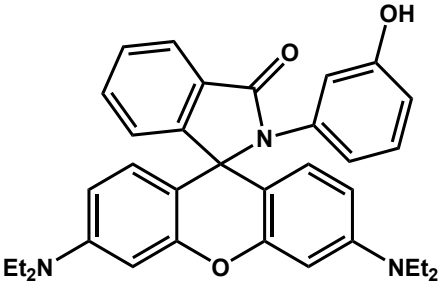	H_2O : ACN = (1 : 10)	Colorimetric and fluorometric response	Within 20 sec. Liquid phase	28

10	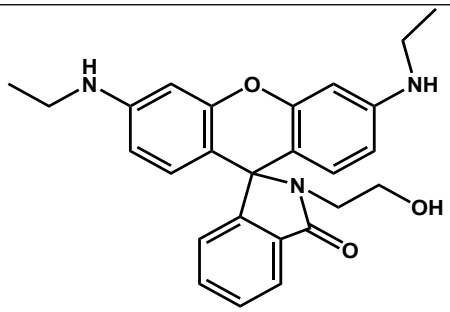	DMF containing 3 % TEA	Colorimetric and fluorometric response	Within 30 sec. Both vapour and liquid phase	29
11	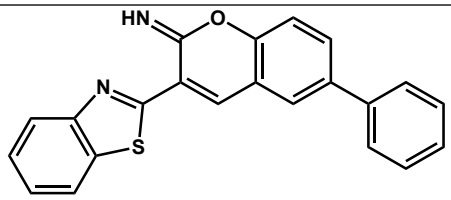	H_2O : ACN = (1 : 1)	Colorimetric and fluorometric response	Within 10 sec. Both vapour and liquid phase	30
12	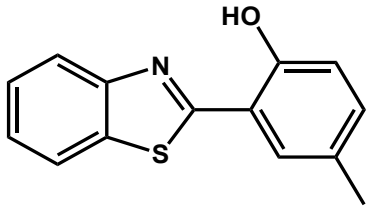	ACN	Colorimetric and fluorometric response.	Within 6 sec. Both vapour and liquid phase	31
13	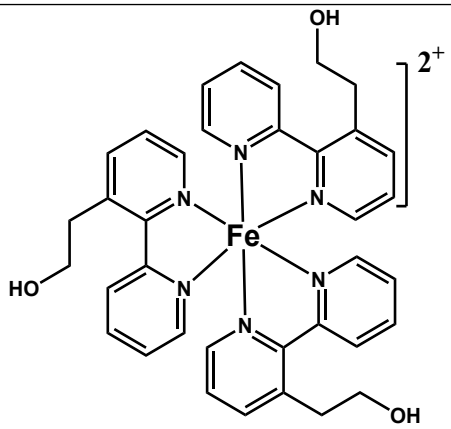	ACN	Colorimetric technique	10 min. Both vapour and liquid phase	32

14	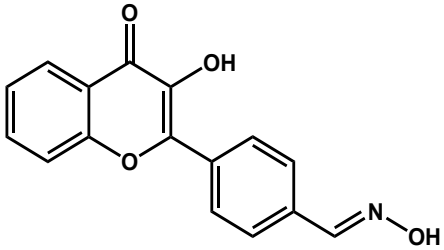	Methanol	Fluorometric response	90 sec. Both vapour and liquid phase	33
15	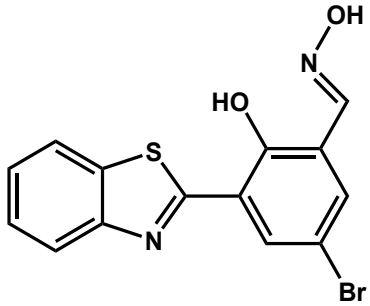	DMF	Colorimetric and fluorometric response.	Within 20 sec. Both vapour and liquid phase	34
16	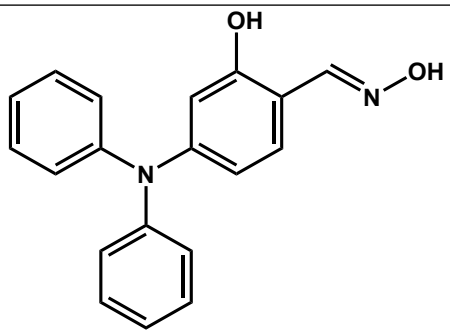	H_2O : ACN = (6 : 4)	Colorimetric and fluorometric response.	Within 1 min Both vapour and liquid phase	35
17	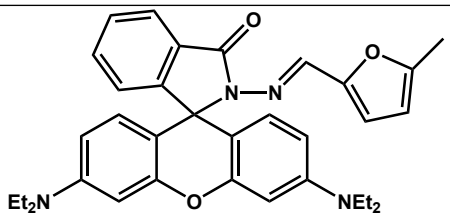	H_2O : ACN = (1 : 1)	Colorimetric and fluorometric response	9 min. Liquid phase	36

18	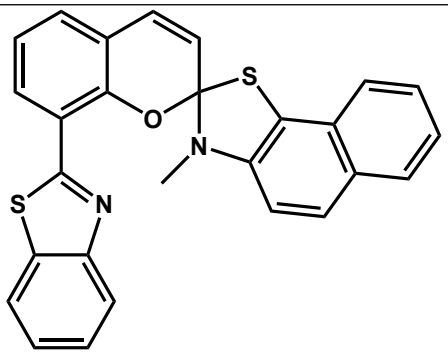	DMSO : HEPES (3 : 7)	Colorimetric and fluorometric response	Within 1 min. Both vapour and liquid phase	37
19	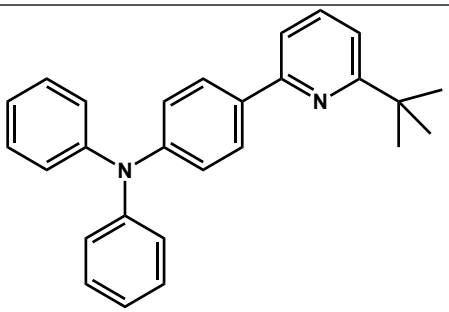	THF	Colorimetric and fluorometric (quenching) response	25 sec. Both vapour and liquid phase	38
20	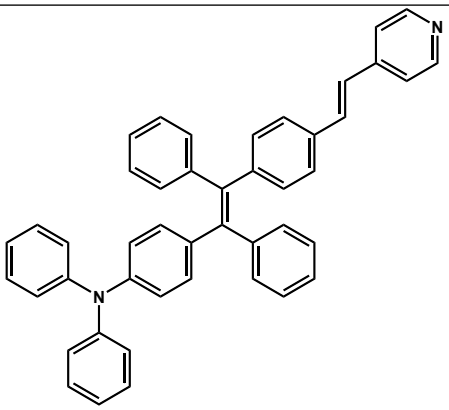	Only vapour phase	Ratiometric AIE fluorometric response	30 sec. Both vapour and liquid phase	39
21	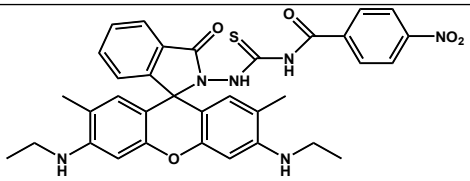	DMF : Water = 1 : 1 with 3 % TEA	Colorimetric and fluorometric response	Within few minutes. Both vapour and liquid phase	40

22	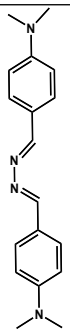	THF solution	Colorimetric and fluorometric response	5 min. Both vapour and liquid phase	41
23	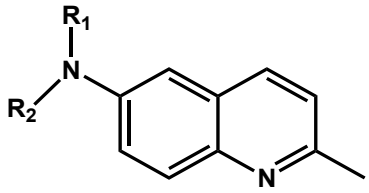	DMSO : ACN (1 : 99)	Colorimetric and fluorometric response	Within 100 sec. Both vapour and liquid phase	42
24	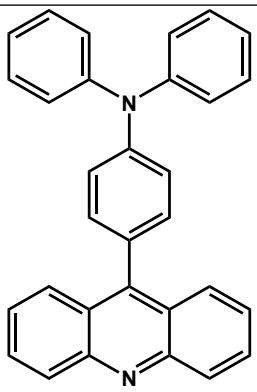	DCM	Colorimetric and fluorometric response	1 sec. Both vapour and liquid phase	43
25	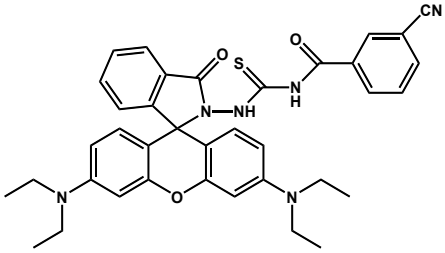	ACN containing 3 % TEA	Colorimetric and fluorometric response	280 sec. Both vapour and liquid phase	44
26	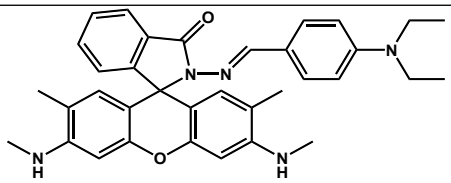	H_2O : EtOH (1 :	Colorimetric and	Within 100 sec	45

		1)	fluorometric response	Both vapour and liquid phase	
27	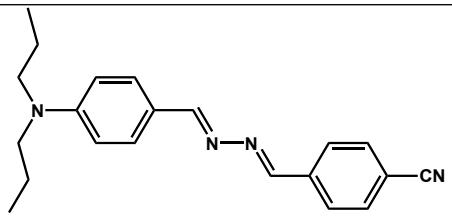	THF : H_2O = (3 : 7)	Colorimetric and fluorometric response.	Within 20 sec Both vapour and liquid phase	46
28	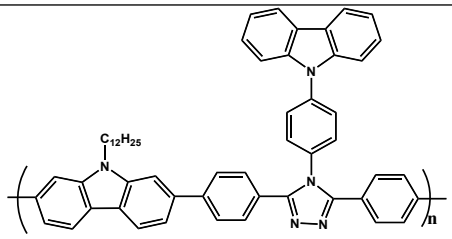	THF	Colorimetric and fluorometric response.	Within 5 sec. Both vapour and liquid phase	47
29	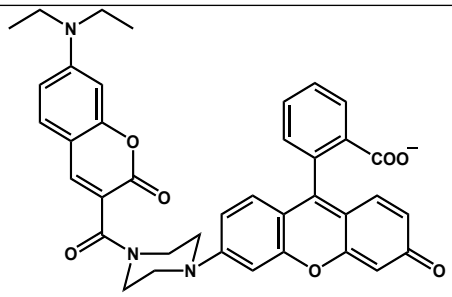	DMF	Fluorometric response.	Within 1 min. Both vapour and liquid phase	48

30	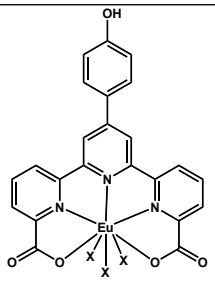	ACN	Fluorometric response.	Liquid phase	49
31	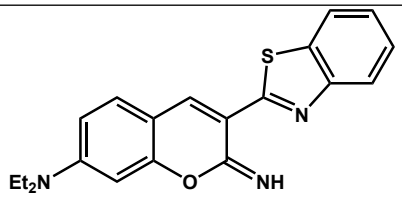	H_2O : DMF = (1 : 1)	Fluorometric response.	Within 10 sec.	50
32	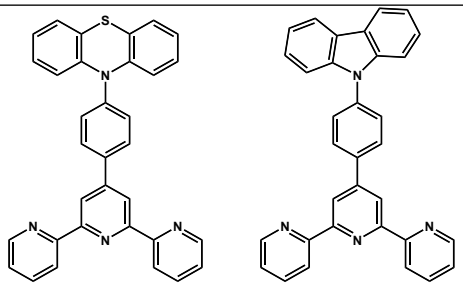	THF	Colorimetric and fluorometric response	Within 5 sec. Both vapor and liquid phase	51

Table S2. X-ray crystallographic data of 1-4.

Parameters	1	2	3	4
Molecular formula	$C_{21}H_{26}NO_4V$	$C_{23}H_{29}N_2O_4V$	$C_{22}H_{28}NO_4V$	$C_{28}H_{31}N_2O_4V$
Molecular weight	407.37	448.42	421.39	510.49
Temperature (K)	295	100 (2)	295	100 (2)
Crystal system	Orthorhombic	Orthorhombic	Monoclinic	Orthorhombic
Space group	$P2_12_12_1$	$P2_12_12_1$	C2	$P2_12_12_1$
Crystal colour	Red	Brown	Red	Brown
a (Å)	8.3617(12)	8.4626(5)	20.070(2)	6.9728(5)
b (Å)	9.8925(16)	11.4719(7)	8.2(8)	16.9243(13)
c (Å)	25.026(4)	22.4492(15)	15.4395(16)	21.2573(15)
α (º)	90	90	90	90
β (º)	90	90	123.721(6)	90
γ (º)	90	90	90	90
Volume ($Å^3$)	2070.1(6)	2179.4(2)	2113.4(4)	2508.6(3)
Z	4	4	4	4
Density (g/cm^3)	1.307	1.367	1.324	1.352
μ mm^{-1}	0.504	0.487	0.496	0.432
F(000)	856.0	944	888.0	1072
Crystal size (mm^3)	0.42 × 0.22 × 0.05	0.323 × 0.184 × 0.06	0.35 × 0.12 × 0.04	0.93 x 0.16 x 0.06
2θ range for data collection	4.42 to 50	5.078 to 61.39	4.88 to 61.21	4.526 to 64.176
Reflections collected	65837	136998	55930	30519
Independent reflections R_{int} R_{σ}	3630 0.0897 0.0326	6774 0.0777 0.0234	6508 0.1129 0.0580	8730 0.1105 0.1112
Data/restraints/ parameters	3630/0/249	6477/0/277	6508/1/258	8730/0/321
Goodness of fit on F^2	1.163	1.060	1.040	0.931
$R1(F_0)$, $wR2(F_0)$ (I≥ 2 σ(*I*))	0.0448 0.1044	0.0260 0.0634	0.0390 0.0854	0.0616 0.1505
$R1(F_0^2)$, $wR2(F_0^2)$ (all data)	0.0743 0.1263	0.0307 0.0665	0.0705 0.1017	0.0877 0.1684
Largest diffraction peak/hole / e $Å^{-3}$	0.23/-0.47	0.28/-0.37	0.20/-0.33	0.98/-0.85
Flack parameter	0(11)	0.019(4)	0.017(9)	0.07(2)
CCDC No.	2179517	2118218	2179407	2118220

Table S3. Selected bond distances and bond angles in 1-4.

Bonds	Bond distances (Å)			
	1	2	3	4
V1-O4	1.597	1.611	1.599	1.603
V1-O1	1.803	1.809	1.789	1.813
V1-O2	1.791	1.817	1.798	1.799
V1-O3	1.778	1.79	1.791	1.803
V1-N	2.408	2.37	2.408	2.408
C15-N	1.481	1.489	1.487	1.490
C7-N	1.483	1.485	1.491	1.495
C8-N	1.489	1.48	1.480	1.483
C1-O1	1.372	1.357	1.366	1.355
C14-O2	1.369	1.354	1.362	1.368
Bonds angles	Bond angles			
O1-V1-O4	97.85	98.87	100.83	98.68
O1-V1-O2	116.59	117.01	116.12	113.17
O1-V1-O3	119.78	118.39	118.73	121.75
O2-V1-O3	116.89	118.37	118.12	117.46
O2-V1-O4	100.34	99.26	98.24	100.77
O3-V1-O4	97.95	96.97	97.62	97.30
O4-V1-N	174.87	174.32	174.31	174.71
O3-V1-N	77.07	77.37	76.72	77.48
O2-V1-N	83.18	83.19	84.19	82.55

O1-V1-N	83.67	84.45	84.06	83.59

Table S4. TD-DFT calculated spin allowed electronic transitions of 1 in acetonitrile solvent.

Important orbital excitations	**Oscillator frequency (*f*)**	**λ, nm**
H-1 → L (12 %) H → L (78 %) H → L+1 (7 %)	0.0249	460
H-1 → L+1 (26 %) H → L+1 (68 %) H → L (4 %)	0.0404	439
H-1 → L (35 %) H-1→ L+1 (41 %) H → L (15 %) H → L+1 (7 %)	0.1122	434
H-1 → L (47 %) H-1→ L+1 (30 %) H → L+1 (14 %) H-1 → L+2 (2 %)	0.0504	410

Table S5. X-ray crystallographic data of H_3L_1, H_3L_2, and H_3L_4.

Parameters	H_3L_1	H_3L_2	H_3L_4
Molecular formula	$C_{63}H_{89}N_3O_{10}$	$C_{63}H_{89}N_3O_{10}$	$C_{56}H_{70}N_4O_7$
Formula weight	1048.37	1048.37	911.16
Temperature (K)	298(2)	100(2)	100(2)
Crystal system	monoclinic	monoclinic	monoclinic
Space group	$P2_1$	$P2_1$	$P2_1$
Crystal colour	Colourless	Colourless	Colourless
a (Å)	10.9618(8)	10.8179(2)	12.4889(7)
b (Å)	21.0542(14)	20.9974(5)	7.0833(4)
c (Å)	14.0676(9)	13.8796(2)	28.1105(16)
α (º)	90	90	90
β (º)	111.390(2)	112.673(10)	93.256(2)
γ (º)	90	90	90
Volume ($Å^3$)	3023.1(4)	2909.08(10)	2482.7(3)
Z	2	2	2
Density (g/cm^3)	1.152	1.197	1.219
μ mm^{-1}	0.077	0.08	0.080
F(000)	1136	1136.0	980.0
Crystal size (mm^3)	0.34 × 0.18 × 0.05	0.55 × 0.34 × 0.08	0.65 × 0.18 × 0.1
2θ range for data collection	3.88 to 52	3.88 to 52	3.64 to 52
Reflections collected	57042	23464	46616
Independent reflections R_{int} R_{sigma}	11894 0.0905 0.0732	9607 0.0368 0.0452	9753 0.0680 0.0496
Data/restraints/parameters	11894/2/719	9607/3/715	9753/1/626
Goodness of fit on F^2	1.039	1.024	1.04
R1(F_0), *wR*2(F_0) (I≥ 2 σ(*I*))	0.0545 0.1200	0.0365 0.0881	0.0476 0.1241
R1(F_0^2), *wR*2(F_0^2) (all data)	0.1112 0.1525	0.0394 0.0902	0.05 0.1266
Largest diffraction peak/hole / e $Å^{-3}$	0.15/-0.17	0.17/-0.17	0.42/-0.27
CCDC No.	2179411	2179413	2179536

Notes and references

1 G. M. Sheldrick, SADABS, Empirical Absorption Correction Program, University of Göttingen, Göttingen, Germany, 1997.

2 G. M. Sheldrick, SAINT 5.1 ed., Siemens Industrial Automation Inc., Madison, WI, 1995.

3 G. M. Sheldrick, SHELXTL Reference Manual: Version 5.1, Bruker AXS, Madison, WI, 1997.

4 L. J. Farrugia, ORTEP-3 for Windows; University of Glasgow: Glasgow, Scotland, 1997.

5 Gaussian 09, Revision D.01, M. J. Frisch, G. W. Trucks, H. B. Schlegel, G. E. Scuseria, M. A. Robb, J. R. Cheeseman, G. Scalmani, V. Barone, B. Mennucci, G. A. Petersson, H. Nakatsuji, M. Caricato, X. Li, H. P. Hratchian, A. F. Izmaylov, J. Bloino, G. Zheng, J. L. Sonnenberg, M. Hada, M. Ehara, K. Toyota, R. Fukuda, J. Hasegawa, M. Ishida, T. Nakajima, Y. Honda, O. Kitao, H. Nakai, T. Vreven, J. A. Montgomery, Jr., J. E. Peralta, F. Ogliaro, M. Bearpark, J. J. Heyd, E. Brothers, K. N. Kudin, V. N. Staroverov, R. Kobayashi, J. Normand, K. Raghavachari, A. Rendell, J. C. Burant, S. S. Iyengar, J. Tomasi, M. Cossi, N. Rega, J. M. Millam, M. Klene, J. E. Knox, J. B. Cross, V. Bakken, C. Adamo, J. Jaramillo, R. Gomperts, R. E. Stratmann, O. Yazyev, A. J. Austin, R. Cammi, C. Pomelli, J. W. Ochterski, R. L. Martin, K. Morokuma, V. G. Zakrzewski, G. A. Voth, P. Salvador, J. J. Dannenberg, S. Dapprich, A. D. Daniels, Ö. Farkas, J. B. Foresman, J. V. Ortiz, J. Cioslowski, and D. J. Fox, *Gaussian 09* (Gaussian, Inc., Wallingford CT, 2009).

6 J. P. Perdew, *Phys. Rev. B.,* 1986, **33,** 8822-8824.

7 J. P. Perdew and A. Zunger, , *Phys. Rev. B.,* 1981, **23,** 5048–5079.

8 S. H, Vosko, L. Wilk and M. Nusair, *Can. J. Phys.,* 1980, **58,** 1200–1211.

9 M. Dolg, M. Wedig, H. Stoll and H. Preuss, *J. Chem. Phys.,* 1987, **86,** 866-872.

10 J. M. L. Martin and A. Sundermann, *J. Chem. Phys.,* 2001, **114,** 3408-3420.

11 R. Ditchfield, W. J. Hehre and J. A. Pople, *J. Chem. Phys.,* 1971, **54,** 724-728.

12 P. C. Hariharan and J. A. Pople, *Theor. Chim. Acta.,* 1973, **28,** 213-222.

13 W. J. Hehre, R. Ditchfield and J. A. Pople, *J. Chem. Phys.,* 1972, **56,** 2257-2261.

14 J. Tomasi, B. Mennucci and R. Cammi, *Chem. Rev.,* 2005, **105,** 2999-3094.

15 GaussView, Version 5, Roy Dennington, Todd Keith, John Millam, Semichem Inc. Shawnee Mission KS. 2009.

16 Skripnikov, L. V. C.; Chemissian, v.4.0; Leonid V. Skripnikov: St. Petersburg, Russia, 2005.

17 N. M. O'Boyle, A. L. Tenderholt and K. M. Langner, *J. Comp. Chem.,* 2008, **29,** 839-845.

18 R. R. Nair, A. Paul, M. Raju, E. Suresh, D. N. Srivastava and P. B. Chatterjee, *Sens. Actuators. B,* 2017, **253,** 213-223.

19 L. Chen, H. Oh, D. Wu, M. H. Kim and J. Yoon, *Chem. Commun.,* 2018, **54,** 2276–2279.

20 R. R. Nair, M. Raju, S. Bhai, I. H. Raval, S. Halder and B. Ganguly, P. B. Chatterjee, *Analyst,* 2019, **144,** 5724-5737.

21 A. M. Costero, S. Gil, M. Parra, P. M. E. Mancini, R. Martínez-Máñez, F. Sancenón and S. Royo, *Chem. Commun.,* 2008, 6002–6004.

22 S. Han, Z. Xue, Z. Wang and T. Bin Wen, *Chem. Commun.,* 2010, **46,** 8413–8415.

23 X. Wu, Z. Wu and S. Han, *Chem. Commun.,* 2011, **47,** 11468–11470.

24 Z. Wu, X. Wu, Y. Yang, T. Bin Wen and S. Han, *Bioorganic Med. Chem. Lett.,* 2012, **22,** 6358–6361.

25 S. Goswami, A. Manna and S. Paul, *RSC Adv.,* 2014, **4,** 21984–21988.

26 M. Gupta and H. Lee, *Sens. Actuator B Chem.,* 2017, **242,** 977–982.

27 Y. J. Jang, S. V. Mulay, Y. Kim, P. Jorayev and D. G. Churchill, *New J. Chem.,* 2017, **41,** 1653–1658.

28 H. S. Sarkar, A. Ghosh, S. Das, P. K. Maiti, S. Maitra, S. Mandal and P. Sahoo, *Sci. Rep.,* 2018, **8,** 3402.

29 G. Heo, R. Manivannan, H. Kim and Y. A. Son, *Dyes Pigments,* 2019, **171,** 107712.

30 L. Patra, P. Ghosh, S. Das, S. Gharami, N. Murmu and T. K. Mondal, *J. Photochem. Photobiol. A Chem.,* 2020, **388,** 112188.

31 X. Hu, H. Zeng, T. Chen, H. Q. Yuan, L. Zeng and G. M. Bao, *Sens. Actuator B Chem.,* 2020, **319,** 128282.

32 L. Ordronneau, A. Carella, M. Pohanka and J. P. Simonato, *Chem. Commun.,* 2013, **49,** 8946–8948.

33 T. Qin, Y. Huang, K. Zhu, J. Wang, C. Pan, B. Liu and L. Wang, *Anal. Chim. Acta.,* 2019, **1076,** 125–130.

34 U. N. Guria, K. Maiti, S. S. Ali, A. Gangopadhyay, S. K. Samanta, K. Roy, D. Mandal and A. K. Mahapatra, *Chem. Selct.* **2020**, 5, 3770–3777.

35 S. S. Ali, A. Gangopadhyay, A. K. Pramanik, U. N. Guria, S. K. Samanta and A. K. Mahapatra, *Dyes Pigments,* 2019, **170,** 107585.

36 A. J. Weerasinghe, C. Schmiesing and E. Sinn, *Tetrahedron,* 2011, **67,** 2833–2838.

37 A. K. Mahapatra, K. Maiti, S. K. Manna, R. Maji, S. Mondal, C. Das Mukhopadhyay, P. Sahoo and D. Mandal, *Chem. Commun.,* 2015, **51,** 9729–9732.

38 J. Yao, Y. Fu, W. Xu, T. Fan, Y. Gao, Q. He, D. Zhu, H. Cao and J. Cheng, *Anal. Chem.,* 2016, **88,** 2497–2501.

39 S. Huang, Y. Wu, F. Zeng, L. Sun and S. Wu, *J. Mater. Chem. C,* 2016, **4,** 10105–10110.

40 H. S. So, S. Angupillai and Y. A. Son, *Sens. Actuator B Chem.,* 2016, **235,** 447-456.

41 Y. Fu, J. Yu, K. Wang, H. Liu, Y. Yu, A. Liu, X. Peng, Q. He, H. Cao and J. Cheng, *ACS Sensors,* 2018, **3,** 1445–1450.

42 Y. C. Cai, C. Li and Q. H. Song, *ACS Sensors,* 2017, **2,** 834–841.

43 X. Li, Y. Lv, S. Chang, H. Liu, W. Mo, H. Ma, C. Zhou, S. Zhang and B. Yang, *Anal. Chem.,* 2019, **91,** 10927–10931.

44 S. Li, Y. Zheng, W. Chen, M. Zheng, H. Zheng, Z. Zhang, Y. Cui, J. Zhong and C. Zhao, *Molecules,* 2019, **24,** 827.

45 K. C. Behera and B. Bag, *Chem. Commun.,* 2020, **56,** 9308–9311.

46 M. Sathiyaraj and V. Thiagarajan, *RSC Adv.,* 2020, **10,** 25848–25855.

47 P. Zheng, A. Abdurahman, G. Liu, H. Liu, Y. Zhang and M. Zhang, *Sens. Actuator B Chem.,* 2020, **322,** 128611.

48 W. Xuan, Y. Cao, J. Zhou and W. Wang, *Chem. Commun.,* 2013, **49,** 10474–10476.

49 K. Gupta and A. K. Patra. *ACS Sensors* **2020**, *5*, 1268–1272.

50 M. S. J. Khan, Y. Wang, M. O. Senge, Y. Peng. *J. Hazard. Mater.* **2018,** *342,* 10-19.

51 P. Zheng, Z. Cui, H. Liu, W. Cao, F. Li, M. Zhang, *J. Hazard. Mater.* **2021,** *415,* 125619.